Lappeenranta
University of Technology

Idrissa S. Amour

VARIATIONAL ENSEMBLE KALMAN FILTERING APPLIED TO DATA ASSIMILATION PROBLEMS IN COMPUTATIONAL FLUID DYNAMICS

Thesis for the degree of Doctor of Science (Technology) to be presented with due permission for public examination and criticism in Auditorium 2310 at Lappeenranta University of Technology, Lappeenranta, Finland on the 15th of August, 2016, at 12:00 pm.

Acta Universitatis
Lappeenrantaensis 707

Supervisor Associate Professor, PhD Tuomo Kauranne
LUT School of Engineering Science
Lappeenranta University of Technology
Finland

Reviewers Professor, PhD Hiroshi Suito
Graduate School of Environmental and Life Science
Okayama University
Japan

PhD Alexey Penenko
Institute of Computational Mathematics and Mathematical Geophysics
Siberian Branch of Russian Academy of Sciences
Russia

Opponent Professor, PhD Hiroshi Suito
Graduate School of Environmental and Life Science
Okayama University
Japan

ISBN 978-952-265-979-8
ISBN 978-952-265-980-4 (PDF)
ISSN 1456-4491
ISSN-L 1456-4491

Lappeenrannan teknillinen yliopisto
Yliopistopaino 2016

Abstract

Idrissa S. Amour
VARIATIONAL ENSEMBLE KALMAN FILTERING APPLIED TO DATA ASSIMILATION PROBLEMS IN COMPUTATIONAL FLUID DYNAMICS
Lappeenranta, 2016
87 p.
Acta Universitatis Lappeenrantaensis 707
Diss. Lappeenranta University of Technology
ISBN 978-952-265-979-8, ISBN 978-952-265-980-4 (PDF), ISSN 1456-4491, ISSN-L 1456-4491

One challenge on data assimilation (DA) methods is how the error covariance for the model state is computed. Ensemble methods have been proposed for producing error covariance estimates, as error is propagated in time using the non-linear model. Variational methods, on the other hand, use the concepts of control theory, whereby the state estimate is optimized from both the background and the measurements. Numerical optimization schemes are applied which solve the problem of memory storage and huge matrix inversion needed by classical Kalman filter methods. Variational Ensemble Kalman filter (VEnKF), as a method inspired the Variational Kalman Filter (VKF), enjoys the benefits from both ensemble methods and variational methods. It avoids filter inbreeding problems which emerge when the ensemble spread underestimates the true error covariance. In VEnKF this is tackled by resampling the ensemble every time measurements are available. One advantage of VEnKF over VKF is that it needs neither tangent linear code nor adjoint code.

In this thesis, VEnKF has been applied to a two-dimensional shallow water model simulating a dam-break experiment. The model is a public code with water height measurements recorded in seven stations along the 21.2 m long 1.4 m wide flume's mid-line. Because the data were too sparse to assimilate the 30×171 model state vector, we chose to interpolate the data both in time and in space. The results of the assimilation were compared with that of a pure simulation. We have found that the results revealed by the VEnKF were more realistic, without numerical artifacts present in the pure simulation.

Creating a wrapper code for a model and DA scheme might be challenging, especially when the two were designed independently or are poorly documented. In this thesis we have presented a non-intrusive approach of coupling the model and a DA scheme. An external program is used to send and receive information between the model and DA procedure using files. The advantage of this method is that the model code changes needed are minimal, only a few lines which facilitate input and output. Apart from being simple to coupling, the approach can be employed even if the two were written in different programming languages, because the communication is not through code. The non-intrusive approach is made to accommodate parallel computing by just telling the control program to wait until all the processes have ended before the DA procedure is invoked. It is worth mentioning the overhead increase caused by the approach, as at every assimilation cycle both the model and the DA procedure have to be initialized. Nonetheless, the method can be an ideal approach for a benchmark platform in testing DA methods.

The non-intrusive VEnKF has been applied to a multi-purpose hydrodynamic model COHERENS to assimilate Total Suspended Matter (TSM) in lake Säkylän Pyhäjärvi. The lake has an area of

154 km^2 with an average depth of 5.4 m. Turbidity and chlorophyll-a concentrations from MERIS satellite images for 7 days between May 16 and July 6 2009 were available. The effect of the organic matter has been computationally eliminated to obtain TSM data. Because of computational demands from both COHERENS and VEnKF, we have chosen to use 1 km grid resolution. The results of the VEnKF have been compared with the measurements recorded at an automatic station located at the North-Western part of the lake. However, due to TSM data sparsity in both time and space, it could not be well matched. The use of multiple automatic stations with real time data is important to elude the time sparsity problem. With DA, this will help in better understanding the environmental hazard variables for instance.

We have found that using a very high ensemble size does not necessarily improve the results, because there is a limit whereby additional ensemble members add very little to the performance. Successful implementation of the non-intrusive VEnKF and the ensemble size limit for performance leads to an emerging area of Reduced Order Modeling (ROM). To save computational resources, running full-blown model in ROM is avoided. When the ROM is applied with the non-intrusive DA approach, it might result in a cheaper algorithm that will relax computation challenges existing in the field of modelling and DA.

Keywords: Dam-break, data assimilation, COHERENS, ensemble methods, forecasts, Kalman filter, non-intrusive algorithm, total suspended matter, variational ensemble Kalman filter, variational methods

Preface

It has been a great pleasure to carryout the work of this Doctoral thesis at the School of Engineering Science of Lappeenranta University of Technology (LUT). This work has been primarily funded by the World Bank Project of the University of Dar es Salaam (UDSM) and staff development programme of UDSM. I would also like to express my gratitude to the LUT for financial assistance during the entire period of this work.

I would like first to express my gratitude to my supervisor Professor Tuomo Kauranne whose supervision throughout this work was encouraging and motivating. There were many hard times on the way, but Tuomo has neither gave up nor shown any disappointment in my progress. I would also like to thank Professor Heikki Haario of LUT who has been actively not only advising but also supporting what we have been doing, his advice and support were always useful and important.

My special thanks go to Professor Hiroshi Suito and PhD Alexey Penenko for their good work in reviewing the manuscript. Of course the shape and relevance of this thesis would not be possible without their constructive and critic arguments during the reviewing process.

Many people have contributed in successful completion of this work, I would like to appreciate special contributions from my colleagues Antti Solonen, Alexander Bibov and Zubeda Mussa. Their contributions not only added the quality of the thesis but also gave me good teamwork experience.

It is worth also to thank a group of people who helped in setting a COHERENS model and answer my inquiries for lake Säkylän Pyhjärvi's matters. To mention few of them are Janne Ropponen and Olli Malve of SYKE, Juhani Saastamoinen of Arbonaut Oy and Akiko Mano.

Life in foreign country might be challenging, however with the presence of good friends this challenge has not been a problem. Thanks to Doctoral students colleagues Almasi M., David K., Gasper M., Isambi M., Miika T., Pendo K. and Zubeda M. Miika has been very useful in assisting with Finnish life matters; for e.g. winter driving difficulty and trick to defrost frozen wind shield washer.

Family friends have been very important for me and my family here in Lappeenranta. Without these family friends life could be very different and boring. I would like to thank these families for their generous friendship and love they have shown us; Cesar I., Issa D. and their families and Tufairi K.

My family has been a good companion throughout my work. In fact, I have been working together with my children during their babyhood. Thanks to them; Maryam, Ahmad, Meiya and Adila. It will be a mistake not to mention my lovely wife Awena, she has been constantly supporting and encouraging in my course. Thanks to my mother Maryam who visited us and got a chance to teach our children home Swahili life. Thank you mother and father for your generosity, love and support.

Lappeenranta, June 2016

Idrissa S. Amour

LIST OF THE ORIGINAL ARTICLES

During the work of this thesis, the following three original refereed articles/manuscripts submitted in scientific journals.

I **A. Solonen, H. Haario, J. Hakkarainen, H. Auvinen, I. Amour and T. Kauranne**, Variational Ensemble Kalman Filtering using Limited Memory BFGS, *Electronic Transaction on Numerical Analysis*, 39, 271–285, 2012.

II **I. Amour, Z. Mussa, A. Bibov and T. Kauranne**, Using ensemble data assimilation to forecast hydrological flumes, *Nonlinear processes in Geophysics*, 20, 955–964, 2013.

III **I. Amour and T. Kauranne**, Data assimilation with 3D and 2D blackbox models: Variational Ensemble Kalman Filtering in COHERENS, *International Journal for Numerical Methods in Fluids*, 2016 (Submitted).

1D	One-Dimension
2D	Two-Dimension
3D	Three-Dimension
3D-Var	Three Dimensional variational method
4D-Var	Three Dimensional variational method
BFGS	Broyden-Fletcher-Goldfarb-Shanno
CFL	Courant-Friedrichs-Levy
CMC	Canadian Meteorological Center
COHERENS	Coupled Hydrodynamical-Ecological Model for Regional and Shelf Seas
DA	Data Assimilation
DASWE	Depth Averaged Shallow Water Equations
ECMWF	European Centre for Medium-Range Weather Forecasts
EKF	Extended Kalman Filter
EnKF	Ensemble Kalman Filter
ETKF	Ensemble Transform Kalman Filter
KF	Kalman Filter
LBFGS	Limited memory BFGS
MOD_FreeSurf2D	A MATLAB Surface Fluid Flow Model for Rivers and Streams
UKMO	United Kingdom Meteorological Office
RMSE	Root Mean Square Error
SREnKF	Square Root Ensemble Kalman Filter
SYKE	Finnish Environmental Institute
TSM	Total Suspended Matter
VEnKF	Variational Ensemble Kalman Filter
VKF	Variational Kalman Filter
WRF	Weather Research and Forecasting

CHAPTER I

Introduction

1.1 Background and motivation

In numerical models of continuous physical processes, errors emerge either due to an incorrect model formulation or excessively simplified physics applied to the model. These errors must be accounted for and, when possible, corrected with other available information. This process is known as data assimilation and the rectifying information is contained in measurements. This can also be seen as a systematic way of combining a model forecast with measurements, which in many cases are sparse in space and limited in time. Traditionally, data assimilation has been mainly applied to weather forecasting. However, there is an increasing number of data assimilation applications in other modeling problems, such as in oceanography, hydrology, geophysics and engineering.

The history of data assimilation goes back to the late 1940s and 1950s (see e.g: Panofsky (1949); Charney et al. (1950); Bergthórssonz and Döös (1955)). Since then several sophisticated methods have been proposed. Statistics of the model forecast analysis using available measurements have been well presented using the Kalman Filter (KF) in Kalman (1960), however limited to linear models only. The use of the Extended Kalman Filter (EKF) has best extended estimates to non-linear model forecasts using linearization techniques to nonlinear model and observation operators. Practical use of the EKF in large-scale higher dimensional problems has been challenging with two concerns. It is computationally expensive, as it is necessary need to invert huge matrices of order of 10^7 by 10^7 in KF algorithm. But also because of the difficulty to implement linearization of the model operator. The Ensemble Kalman Filter (EnKF), introduced by Evensen (1994) has come up with the solution to replace linearization of the model operator. In this approach the model error covariance is propagated by the non-linear evolution model using ensemble members. Different techniques which find the analysis by solving an optimization problem have also been proposed. Three-dimensional variational assimilation (3D-Var) and four-dimensional variational assimilation (4D-Var) are good examples in this category. The latter method finds the analysis by scanning over measurements back and forth in time, which makes it superior to 3D-Var, but difficult to implement.

The main challenge in data assimilation is on how to estimate the error covariance of the analysis. The ensemble Kalman filter method came up with an affordable solution to this problem, that brought growing attention to combining or coupling ensemble methods with variational methods (see e.g. Kauranne (1992); Hunt et al. (2007); Hamill and Snyder (2000); Wang et al. (2008); Clayton et al. (2013); Lorenc et al. (2015)). In this manuscript we present sophisticated applications of

the novel hybrid assimilation methods known as the Variational Ensemble Kalman Filter (VEnKF). The VEnKF was introduced by Solonen et al. (2012) and tested with the Lorenz 95 model and the two-dimensional heat equation model. The performance of any assimilation method should be judged with respect to the quality of the analysis it produces and how computationally cheap it is with large-scale higher dimensional models. The latter is more crucial, since the aim of any method development is to make it operational, otherwise forecasting procedure will have no traction in real time applications. As many other ensemble methods, VEnKF can be smoothly adapted to run in parallel computing environment, which is a great advantage for the future parallel supercomputers in atmospheric model (e.g see in Kauranne (1994)).

The use of any assimilation method in a coupled model system is another challenge. In many cases the documentation of the model code might not be available, or available but not fully detailed. That makes it difficult to make a wrapper code for the assimilation scheme with the model code. Even for a fully documented model code, the cost of making the wrapper code remains very high. In recent work (Nerger and Hiller, 2013; Nerger and Kirchgessner, 2015), it has been shown how to use an offline coupling approach through disk files, which has the advantage that no model code needs to be changed. In the same work of Nerger and Kirchgessner (2015), there is an online coupling approach with minimal change to the model code introduced too. The choice of data assimilation to be embedded in a complex model might be difficult if we can not spend less effort for testing different data assimilation schemes. Browne and Wilson (2015) used MPI to couple an unstructured finite element model of the North sea (TELEMAC) with 114288 state variables with the MPI approach. The advantage of MPI is that no disk files are written (online approach) (Browne and Wilson, 2015), but the model code must be changed to be coupled with the data assimilation scheme, which is not always straightforward.

1.2 Objective of the study

In this thesis we aim to achieve the following:

i. Study the innovation of a robust data assimilation scheme which utilizes the features of ensemble methods for error covariance propagation and a variational method for its analysis estimation with respect to the prior model information and the measurements.

ii. Study both qualitative and quantitative properties of the new hybrid data assimilation method with both 2-dimensional and 3-dimensional hydrodynamic model.

iii. Study non-intrusive implementation of this data assimilation scheme to be easily implemented without any model code change.

iv. Explore and study non-intrusive way of coupling the novel data assimilation method with a large-scale higher dimensional hydrodynamic model.

1.3 Author's contributions

In this thesis, the author has made the following contributions.

i. In the innovation of the Variational Ensemble Kalman filtering, the author participated in the discussion of the development of the novel method. In particular the author made a code for model forecast analysis (forecast skill plots), which appear in the publication of Solonen et al. (2012).

ii. The author used an untested method with real problems, to a real problem of shallow water model, the work appearing in the publication of Amour et al. (2013), where the assimilation of water heights was performed using VEnKF in a dam-break experiment.

iii. The author explored the use of non-intrusive data assimilation schemes to the hydrodynamic model of shallow water and deep oceans (COHERENS), using an wrapper program to manage both the model evolution and the assimilation method.

1.4 Organization of the thesis

This thesis is made of seven chapters. The current first chapter is introducing the study and gives insight of the objectives and the author's contributions. The second chapter gives an overview of data assimilation methods and their properties. The third chapter introduces the Variational Ensemble Kalman filter (VEnKF) method, its algorithm and test cases. The fourth chapter is devoted to the application of the VEnKF to the two-dimensional shallow water model in a dam-break experiment. The fifth chapter introduces a multipurpose hydrodynamic model COHERENS. Chapter six is devoted to the non-intrusive implementation of the data assimilation scheme (VEnKF) and the last chapter, chapter seven, comprises conclusions and discussion of the results of the thesis.

CHAPTER II

Data assimilation

2.1 Brief history

Physical processes are difficult to model. Scientists are struggling to make numerical models of physical processes as accurately as they can, but the danger of incomplete physics representation is always there. Some of the processes are well known, but due to computational limitations, scientists chose to simplify the model. These are examples of sources of errors in the forecasting process. On the other hand the data from measuring instrument contains errors, either due to the person who is reading or the measurement device itself. It is therefore important to combine both models and measurements. This processes is what is called Data assimilation (DA). Data assimilation can simply be understood as a systematic way of combining the information from the model (prior or background) and that from the measurements (data) from measuring device to produce a new state (analysis). Technically, data assimilation assumes some weighted average between the prior and the data, with weights that are inversely proportional to the anticipated error in each (Daley, 1991).

One of the great pioneers in forecasting studies, Richardson (1922), gave unrealistic forecasts for the change in surface pressure over a six-hour period. However, it has been shown that with the same method that Richardson was using, but with smoothed data, the results are realistic (Lynch, 2006). The missing technique for Richardson's work was data assimilation. The history of data assimilation goes back to 1940s when Panofsky was studying the application of hydrodynamic equations to forecasting, and suggested that an initial condition for the problem has to be furnished by the observations at the starting time as long as other variables of the hydrodynamic equations are already known. The method used a third-degree polynomial to fit the wind and pressure fields in an area of order of 10^8 square miles (Panofsky, 1949). Data assimilation has been for a while popular in the fields of meteorology and oceanography, and has been put operational first with the optimal interpolation method (Daley, 1991). Nowadays, data assimilation is applied in a wide range of applications; such as hydrology, geophysics, environment and engineering. In hydrology, for example, data assimilation has been used in an error forecasting procedure (see e.g in Madsen and Skotner (2005); Reichle et al. (2008)). However a common way to apply data assimilation to hydrological models is to update the initial conditions based on the prior and the measurements (see e.g in Amour et al. (2013); Heemink and Metzelaar (1995)). A demonstration of such an assimilation is presented in Figure 2.1

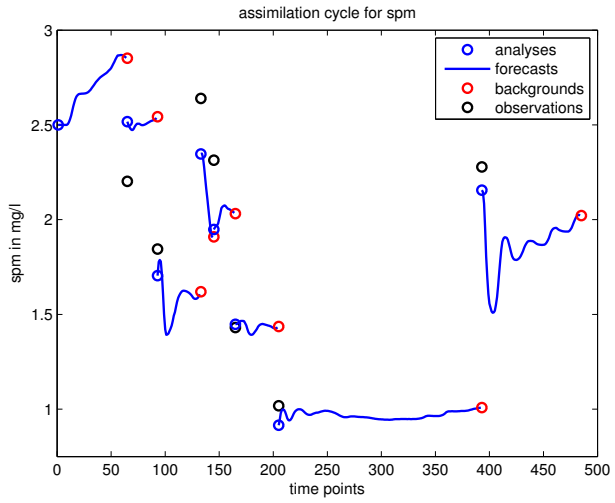

Figure 2.1: Demonstration: An assimilation cycle shown for suspended particular matter (spm), using satellite data in lake Säkylän Pyhäjärvi. Black circles are data points, red circles are the model background, blue circles are state analyses and the blue trajectories are model forecasts.

2.2 Sequential methods

Data assimilation methods can be classified into two categories; sequential methods and variational methods. Sequential methods uses statistical approaches to find an estimate of the whole system by propagating the information forward in time sequentially (Bertino et al., 2003; Evensen, 2009). It is common practice to assume that the model state ξ_{k+1} depends only on ξ_k and the observation Υ_k depends only on the state ξ_k. For the following text, indices $0:k$ stands for a sequence $0, 1, ..., k$. The task is to find the most likely model state trajectory $\xi_{0:k}$ while the model dynamics and measurements are known. In other words, we have to estimate a posterior density $\pi(\xi_{0:k}|\Upsilon_{0:k})$. Sequential methods estimate the posterior density function in a two steps algorithm;

i. A propagation step using model dynamics to get the prior distribution $\pi(\xi_k|\Upsilon_{0:k-1})$, and

ii. An analysis step using the observations Υ_k to update the prior distribution, that gives the posterior distribution $\pi(\xi_k|\Upsilon_{0:k})$,

There are several sequential methods proposed, with main concerns of computing cost, algorithm robustness to non-linear models and robustness to error statistics (e.g see Verlaan and Heemink (2000); Pham (2000); Canizares (1999)). In this manuscript we will mention the most studied sequential methods; Kalman Filter (KF) and its derivatives.

2.2.1 Kalman Filter

Kalman Filter (KF) has first been studied in engineering problems by Kalman. He found that the problem of data assimilation is connected to other problems in control theory (Kalman, 1960). That also gave an opportunity for KF to be adapted to other fields. Before introducing the formulation of the KF, we first consider the relationship between a dynamic model, M, the state vector ξ and the measurements Υ in data assimilation aspects. The Equations (2.1) and (2.2) form an important part for any DA procedure

$$\xi_{k+1} = \mathrm{M}(\xi_k) + \varepsilon_k \tag{2.1}$$
$$\Upsilon_k = \mathrm{K}(\xi_k) + \varepsilon_k^o \tag{2.2}$$

Here ε_k and ε_k^0 are the model and observation error, respectively. In this work we will not derive the KF in its original derivation, but instead we will show how it follows directly from the Bayesian approach as it appears in Haario (2006). We start with the Bayes rule with normalization constant ignored

$$\pi(\xi) = p(\Upsilon|\xi)p(\xi) \tag{2.3}$$

where $\pi(\xi)$ is the posterior distribution, $p(\xi)$ is the prior distribution and $p(\Upsilon|\xi)$ is the likelihood function. Assume a linear model given by

$$\Upsilon = Z\xi + \varepsilon^o \tag{2.4}$$

where Z is the design (observation) matrix extended with 1's in the first column. Assuming again that the measurement error and the prior distribution are Gaussian, with covariances matrices C_{ε^o} and C_{ε^p} respectively, and denoting the prior by ξ_b, then

$$p(\xi) \approx e^{-\frac{1}{2}(\xi-\xi_b)^T C_{\varepsilon^p}^{-1}(\xi-\xi_b)}$$

$$p(\Upsilon|\xi) \approx e^{-\frac{1}{2}(\Upsilon-Z\xi)^T C_{\varepsilon^o}^{-1}(\Upsilon-Z\xi)}$$

Combining the two equations and taking logarithm of both sides, we get

$$-2\log(\pi(b)) = (\Upsilon - Z\xi)^T C_{\varepsilon^o}^{-1}(\Upsilon - Z\xi) + (\xi - \xi_b)^T C_{\varepsilon^p}^{-1}(\xi - \xi_b)$$

This least squares problem can be simplified using a Cholesky decomposition (Haario, 2006). Splitting the covariance matrices gives

$$C_{\varepsilon^o}^{-1} = K_{\varepsilon^o}^T K_{\varepsilon^o} \quad \text{and} \quad C_{\varepsilon^p}^{-1} = K_{\varepsilon^p}^T K_{\varepsilon^p}$$

Substitution provides the new form

$$\begin{aligned} -2\log(\pi(\xi)) &= (K_{\varepsilon^o}\Upsilon - K_{\varepsilon^o}Z\xi)^T(K_{\varepsilon^o}\Upsilon - K_{\varepsilon^o}Z\xi) + (K_{\varepsilon^p}\xi - K_{\varepsilon^p}\xi_b)^T(K_{\varepsilon^p}\xi - K_{\varepsilon^p}\xi_b) \\ &= ||K_{\varepsilon^o}Z\xi - K_{\varepsilon^o}\Upsilon||^2 + ||K_{\varepsilon^p}\xi - K_{\varepsilon^p}\xi_b||^2 \end{aligned}$$

This expression is nothing but the least squares problem $\tilde{\Upsilon} = \tilde{X}\xi$, where

$$\tilde{X} = \begin{bmatrix} K_{\varepsilon^o}Z \\ K_{\varepsilon^p} \end{bmatrix} \quad \text{and} \quad \tilde{\Upsilon} = \begin{bmatrix} K_{\varepsilon^o}\Upsilon \\ K_{\varepsilon^p}\xi_b \end{bmatrix}$$

If we assume the covariance to be distributed with $\mathbf{N}(\mathbf{0}, \mathbf{I})$, then using the least squares solution, we can compute the coefficients $\hat{\xi}$ and its covariance S as follows

$$\hat{\xi} = (\tilde{X}^T\tilde{X})^{-1}\tilde{X}^T\tilde{\Upsilon} \quad \text{and} \quad S = \text{cov}(\hat{\xi}) = (\tilde{X}^T\tilde{X})^{-1}$$

We can then compute

$$\tilde{X}^T\tilde{X} = Z^T K_{\varepsilon^o}^T K_{\varepsilon^o} Z + K_{\varepsilon^p}^T K_{\varepsilon^p} = Z^T C_{\varepsilon^o}^{-1} Z + C_{\varepsilon^p}^{-1}$$
$$\tilde{X}^T\tilde{\Upsilon} = Z^T K_{\varepsilon^o}^T K_{\varepsilon^o} \Upsilon + K_{\varepsilon^p}^T K_{\varepsilon^p} \xi_b = Z^T C_{\varepsilon^p}^{-1} \Upsilon + C_{\varepsilon^p}^{-1} \xi_b$$

Therefore, the values for the estimates $\hat{\xi}$ and S are

$$\hat{\xi} = (Z^T C_{\varepsilon^p}^{-1} \Upsilon + C_{\varepsilon^p}^{-1} \xi_b)^{-1} (Z^T C_{\varepsilon^o}^{-1} Z + C_{\varepsilon^p}^{-1}) \tag{2.5}$$
$$S = (Z^T C_{\varepsilon^o}^{-1} Z + C_{\varepsilon^p}^{-1})^{-1} \tag{2.6}$$

The posterior is Gaussian with mean $\hat{\xi}$ and covariance S, we can write it as

$$-2\log(\pi(\xi)) = (\xi - \hat{\xi})^T S^{-1} (\xi - \hat{\xi}) + c$$

where c is a constant. Modifying Equation (2.6) by putting $\mathbf{I} = C_{\varepsilon^p} C_{\varepsilon^p}^{-1}$, then

$$\begin{aligned} S &= (Z^T C_{\varepsilon^o}^{-1} Z + C_{\varepsilon^p}^{-1})^{-1} C_{\varepsilon^p} C_{\varepsilon^p}^{-1} \\ &= (C_{\varepsilon^p} Z^T C_{\varepsilon^o}^{-1} Z + \mathbf{I})^{-1} ((C_{\varepsilon^p} Z^T C_{\varepsilon^o}^{-1} + \mathbf{I}) C_{\varepsilon^p} - C_{\varepsilon^p} Z^T C_{\varepsilon^o}^{-1} Z C_{\varepsilon^p}) \\ &= C_{\varepsilon^p} - (C_{\varepsilon^p} Z^T C_{\varepsilon^o}^{-1} Z + \mathbf{I})^{-1} C_{\varepsilon^p} Z^T C_{\varepsilon^o}^{-1} Z C_{\varepsilon^p} \end{aligned}$$

factoring C_{ε^p} out in the second term, we then have

$$S = C_{\varepsilon^p} - (Z^T C_{\varepsilon^o}^{-1} Z + C_{\varepsilon^p}^{-1})^{-1} Z^T C_{\varepsilon^o}^{-1} Z C_{\varepsilon^p} \tag{2.7}$$

With algebraic manipulation, one can show that

$$(Z^T C_{\varepsilon^o}^{-1} Z + C_{\varepsilon^p}^{-1})^{-1} Z^T C_{\varepsilon^o}^{-1} = C_{\varepsilon^p} Z^T (Z C_{\varepsilon^p} Z^T + C_{\varepsilon^o})^{-1} \tag{2.8}$$

Let us now define the Kalman Gain matrix G as follows

$$G = C_{\varepsilon^p} Z^T (Z C_{\varepsilon^p} Z^T + C_{\varepsilon^o})^{-1} \tag{2.9}$$

Substituting (2.9) and (2.8) into (2.7), we then get

$$S = C_{\varepsilon^p} - G Z C_{\varepsilon^p} \tag{2.10}$$

Similarly for $\hat{\xi}$, we can show that

$$\hat{\xi} = \xi_b + (Z^T C_{\varepsilon^o}^{-1} Z + C_{\varepsilon^p}^{-1})^{-1} Z^T C_{\varepsilon^p}^{-1} (\Upsilon - Z\xi_b)$$

Substituting the value of G, we then have

$$\hat{\xi} = \xi_b + G(\Upsilon - Z\xi_b) \tag{2.11}$$

In the context of DA, the dynamic linear model M replaces the design matrix Z in (2.9) and observation operator K replaces the design matrix Z in (2.11), then the linear equations would be

$$\xi_k = \mathrm{M}_t\xi_{k-1} + \varepsilon \quad \text{and} \quad \Upsilon_k = \mathrm{K}_k\xi_k + \varepsilon_k^o$$

The covariance, $\mathrm{cov}(\xi_k) = C_{\varepsilon^p}^k$ of the prior can be approximated, with the assumption that the prior covariance error and model error are independent, by

$$C_{\varepsilon^p}^k = \mathrm{cov}(\mathrm{M}_k\xi_{k-1} + \varepsilon) = \mathrm{M}_k C_{\varepsilon^p}^{k-1}\mathrm{M}_k^T + C_\varepsilon$$

where C_ε is the error covariance matrix for the model. Rewriting all the equations, with respect to the linear models defined by model operators M and observation operator K. The collection of formulae (2.12) to (2.16) in that order, form the basic KF algorithm

1. Initialize: $\hat{\xi}_0$ and $\hat{C}_{\varepsilon^p}^0$
2. $1 \leftarrow k$
3. Compute the forecast: $\xi_k = \mathrm{M}_k\hat{\xi}_{k-1}$ (2.12)
4. Compute prior covariance: $C_{\varepsilon^p}^k = \mathrm{M}_k\hat{C}_{\varepsilon^p}^{k-1}\mathrm{M}_k^T + C_\varepsilon^k$ (2.13)
5. Compute Kalman Gain: $G_k = C_{\varepsilon^p}^k\mathrm{K}_k^T(\mathrm{K}_k C_{\varepsilon^p}^k\mathrm{K}_k^T + C_{\varepsilon^o}^k)^{-1}$ (2.14)
6. Update the state estimate: $\hat{\xi}_k = \xi_b + G_k(\Upsilon_k - \mathrm{K}_k\xi_b)$ (2.15)
7. Update posterior covariance: $\hat{C}_{\varepsilon^p}^k = C_{\varepsilon^p}^k - G_k\mathrm{K}_k C_{\varepsilon^p}^k$ (2.16)

GoTo Step 3

where $\widehat{st}$ stands for estimate of the variable st.

Kalman Filter can be regarded as a generalization of the least squares problem, and hence supposed to be optimal for linear models (Kalman, 1960; Evensen, 2009). This suggests that KF might not give the desired results if the model dynamics or the observation operator are non-linear.

2.2.2 Extended Kalman Filter

The Extended Kalman Filter (EKF), is a modified version of the KF in such a way that, it accommodates smooth nonlinear dynamic models. Its adjustments include local linearization of the model dynamics $\mathscr{M}$ and the observation operator $\mathscr{K}$. We shall assume continuous and differentiable model dynamics $\mathscr{M}$. We can treat linearization of the model dynamics $\mathscr{M}$ at the state estimate $\hat{\xi}$ with the help of a Taylor series expansion

$$\mathscr{M}(\xi) = \mathscr{M}(\hat{\xi}) + \frac{\mathscr{M}'(\hat{\xi})}{1!}(\xi - \hat{\xi}) + \frac{\mathscr{M}''(\hat{\xi})}{2!}(\xi - \hat{\xi})^2 + \ldots + \frac{\mathscr{M}^n(\hat{\xi})}{n!}(\xi - \hat{\xi}) + R_n(\xi) \tag{2.17}$$

where R_n is the error term (James et al., 2011). Ignoring higher order derivatives, we get

$$\mathscr{M}(\xi) = \mathscr{M}(\hat{\xi}) + \frac{\mathscr{M}'(\hat{\xi})}{1!}(\xi - \hat{\xi}) \tag{2.18}$$

One can write Equation (2.18) as

$$\mathscr{M}(\xi) = \mathscr{M}'(\hat{\xi})\xi + \mathscr{M}(\hat{\xi}) - \mathscr{M}'(\hat{\xi})\hat{\xi} \tag{2.19}$$

$\mathscr{M}$ has only the first order derivatives and constant terms. It is possible to write $\mathscr{M}'$ as the linear dynamic matrix at the point of estimation. We apply this technique to both model dynamics and the observation mapping to obtain Equations (2.20) and (2.21) which can also be found in various studies (e.g. see Simon (2002); Kauranne (2002); Evensen (2009); Auvinen et al. (2010); Sun et al. (2015)).

$$\mathrm{M}'_k = \left.\frac{\partial \mathscr{M}_k(\xi)}{\partial x_k}\right|_{\xi=\hat{\xi}_{k-1}} \tag{2.20}$$

In a similar way, the derivative estimate for the observation operator $\mathscr{K}$ is given by:

$$\mathrm{K}'_k = \left.\frac{\partial \mathscr{K}_k(\xi)}{\partial x_k}\right|_{\xi=\xi_k} \tag{2.21}$$

The state vector normally consists of multiple variables and therefore it is convenient to express the derivative in the form of a Jacobian matrix (J)

$$J_{\mathrm{M}} = \begin{bmatrix} \frac{\partial \mathscr{M}_1}{\partial x_1} & \frac{\partial \mathscr{M}_1}{\partial x_2} & \dots & \frac{\partial \mathscr{M}_1}{\partial x_n} \\ \frac{\partial \mathscr{M}_2}{\partial x_1} & \dots & \dots & \frac{\partial \mathscr{M}_2}{\partial x_n} \\ \vdots & \dots & \dots & \vdots \\ \frac{\partial \mathscr{M}_n}{\partial x_1} & \frac{\partial \mathscr{M}_n}{\partial x_2} & \dots & \frac{\partial \mathscr{M}_n}{\partial x_n} \end{bmatrix} \tag{2.22}$$

Where J_{M} is the Jacobian matrix for the nonlinear model $\mathscr{M}$. The Jacobian matrix, defined by (2.22) is usually hard to solve analytically and in many cases the numerical approach is the way forward (Sun et al., 2015). For instance, a numerical approach can be used in these derivatives to define a tangent linear code (see, e.g. Le Dimet and Talagrand (1986)). Another approach, however a computationally demanding one, is to apply finite differences in Equations (2.20) and (2.21) (Jiashu and Zutao, 2006; Auvinen et al., 2010).

The EKF is well-known for its good state and covariance estimates, which makes it a standard DA algorithm that is used to test the performance of novel DA methods. Despite its outstanding performance, EKF has never been feasible for large-scale high dimensional model problems, due to its computational demands. In Auvinen et al. (2009), it was suggested to use KF and EKF with minimization algorithms to estimate the covariance matrices in order to address the memory and computational issues related to both filters. One obstacle in EKF is caused by huge matrix inversions and the other one in linearization of model dynamics and observations operators, which are usually computationally expensive. Other potential defect for EKF is that the derivative approximations might introduce significant errors in the state estimate and covariances that may lead to sub-optimal performance and even divergence of the EKF (Evensen, 1992; Gauthier et al., 1993; Wan and Merwe, 2000).

The EKF algorithm is similar to the KF algorithm with the exception that, EKF uses the linearized version of model dynamics $\mathscr{M}$ in Equation (2.13) and a linearized version of the observation operator $\mathscr{K}$ in Equations (2.14) through (2.16). In some cases the linearization of observation operator can be skipped by incorporating the observed variable into the state vector (Kondrashov et al., 2008; Sun et al., 2015; Amour et al., 2013).

2.2.3 Ensemble Kalman Filter

The estimate of a state is characterized by the error covariance estimate, in which case when it is overestimated or underestimated the filter may diverge. The Ensemble Kalman Filter (EnKF) comes with its own fashion of doing this that uses the non-linear model to propagate error covariance using a Monte Carlo approach, where the members of the ensemble are used to represent a specific probability density function (Evensen, 1994; van Leeuwen and Evensen, 1996; Evensen and van Leeuwen, 1996). The idea behind is to overcome the computational demands of EKF in error covariance estimates (Evensen, 1994, 2009), but also to skip the use of a tangent linear code needed by EKF (Evensen, 1994, 1996, 2009). Ensemble members represent separate and independent runs with slightly different initial conditions.

The EnKF algorithm takes similar steps with that of KF. The differences is that the covariance error is estimated by the ensemble instead of the KF formula. The EnKF formulation and algorithm are well presented in various studies, including Evensen (1994); Evensen and van Leeuwen (1996); Houtekamer and Herschel (1998, 2001). As a rule of notation in this thesis, let $\hat{\xi}$ be the state estimate or the first guess of the EnKF, C_{ε^p} denote the error covariance matrix for the estimate and X be a matrix of ensemble members, whose size is $N \times n$, where N is the dimension of the state vector ξ and n is the ensemble size. Then, the ensemble forecast and forecast error covariance at time point k are given by

$$\hat{X}_k^j = \mathscr{M}(X_{k-1}^j) \tag{2.23}$$

$$C_{\varepsilon^p}^k = \frac{(\hat{X}_k - \hat{\xi}_k)(\hat{X}_k - \hat{\xi}_k)^T}{n-1} \tag{2.24}$$

where $\hat{\xi}$ is the mean as defined in Equation (2.27) and $\hat{X}^j$ is the jth ensemble member. The rank of the error covariance matrix C_{ε^p} is clearly less than or equal to the number of ensemble members. The Kalman Gain G is computed in the same way using Equation (2.9). The ensemble members are corrected using measured data in a similar fashion as in Equation (2.15),

$$X_k^j = \hat{X}_k^j + G_k(\Upsilon_k - \mathrm{K}_k\hat{\xi}_k)\ , \quad j = 1\ldots, n \tag{2.25}$$

To optimize the computations, some tricks have been applied by which, there is no need to keep a full matrix C_{ε^p}. Actually we only need the product $C_{\varepsilon^p}\mathrm{K}^T$ in Equation (2.9), thus (as presented in Evensen (1994); Evensen and van Leeuwen (1996); Houtekamer and Herschel (1998, 2001)), we can easily avoid this trouble by computing nested products, as shown in Equation (2.26)

$$C_{\varepsilon^p}^k\mathrm{K}_k^T = \frac{1}{n-1}\sum_{j=1}^{n}(\hat{X}_k^j - \hat{\xi}_k)[\mathrm{K}_k(\hat{X}_k^j - \hat{\xi}_k)]^T \tag{2.26}$$

where

$$\hat{\xi}_k = \frac{1}{n}\sum_{j=1}^{n}\hat{X}_k^j \tag{2.27}$$

Similarly, for the term $\mathrm{K}_kC_{\varepsilon^p}^k\mathrm{K}_k^T$ in Equation (2.9), the product can be computed as a nested product

$$\mathrm{K}_kC_{\varepsilon^p}^k\mathrm{K}_k^T = \frac{1}{n-1}\sum_{j=1}^{n}\mathrm{K}_k(\hat{X}_k^j - \hat{\xi}_k)[\mathrm{K}_k(\hat{X}_k^j - \hat{\xi}_k)]^T \tag{2.28}$$

The size of the ensemble n naturally dictates the error in the solution: the higher the size, the lower the error at a rate proportional to $1/\sqrt{n}$ (Evensen, 1994, 2009). In the sense of covariance error computation and storage, EnKF is more affordable than EKF. It has been successfully put to operational use by the Canadian Meteorological Center to give an ensemble of initial states for the medium-range weather forecast (Houtekamer and Herschel, 2005). Many variants of EnKF have been proposed. One to be mentioned here is the Four-dimensional ensemble Kalman filter. This version has the advantages of using observations that have come earlier than the assimilation time, and therefore can track better the model history with respect to the observations (Hunt et al., 2004).

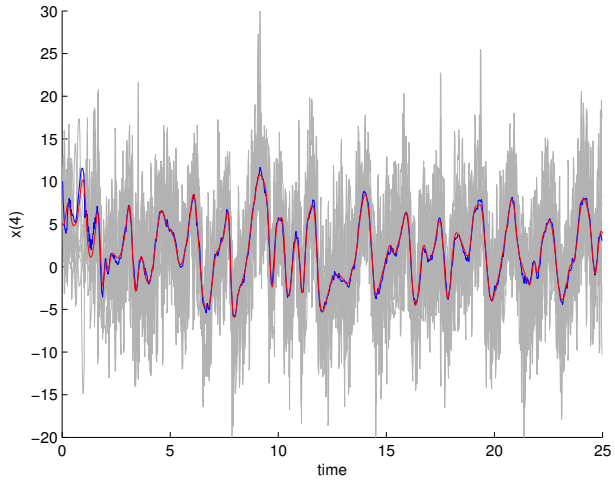

Figure 2.2: Demonstration: Ensemble method type of assimilation for Lorenz 95 model using artificial data obtained by noising the model solution. Vertical axis represents 4th component of the Lorenz 95 model. Red line is the truth, blue line is the forecast and gray lines are the 10 ensemble members used in the assimilation.

One challenge of the EnKF and its variants are their difficulty for setting good initialization for the ensemble members. The filter performance and the estimates are sensitive to the ensemble initialization. EnKF has come under attack on its tendency of losing track for the error covariance estimate over time, which distorts state estimation and, as a result the filter diverges. This property is known as covariance leakage or filter inbreeding and has been examined in several studies (some are: Houtekamer and Herschel (1998); Lorenc (2003); Franssen and Kinzelbach (2008); Li et al. (2009, 2012)). Several measures have been proposed to overcome the filter inbreeding problem, for example; covariance inflation (Hamill et al., 2001; Anderson, 2007; Wang et al., 2007) and an inflation-free iterative EnKF which employs Levenberg-Marquardt scheme to control the optimization process, subsequently this avoids the rank issue associated with classical EnKF (Bocquet and Sakov, 2012). In covariance inflation, both the ensemble and the covariance matrix are scaled using a fixed multiplier (fixed covariance inflation) or scaled with a varying multiplier (adaptive covari-

ance inflation). Houtekamer and Herschel (1998) suggested a two-way EnKF algorithm in which the ensemble is split into two sets; one set is used in assimilation while the other set is used to provide covariance statistics. An obvious drawback of this method is that the filter does not benefit from all ensemble runs but only half of them. In a different context, a technical approach that uses Monte Carlo sampling, where the samples are drawn according to the leading eigenvectors of the covariance matrix has been proposed (Verlaan and Heemink, 1997; Evensen, 2004; Zhang et al., 2007).

2.3 Variational methods

Variational DA methods are based on optimal control theory. A detailed description of optimal control theory can be found for example in Lions (1971). Le Dimet and Talagrand (1986) have shown how to use optimal control theory in problems encountered in meteorology. Optimization is performed on unknown variables or parameters (let us say the model state ξ) by minimizing a known cost function that determines the misfit between the measured data Υ and the model background state $\xi_b$mapped into the observation space by the observation operator. The minimizer from the minimization is used as the new initial state for the model. The cost function has to be minimized numerically with some large-scale unconstrained minimization scheme that uses information from both the function and the gradient. The formulation of variational methods is simple and thus can be easily adapted, with several advantages. Variational methods are equivalent to the optimal linear Kalman Filter for a perfect model (Daley, 1991). In the nonlinear case, the results from variational methods have been proved to be better than their sequential method counterparts as long as the assimilation period does not exceed the validity of the tangent linear approximations (Rabier and Courtier, 1992).

In this section of the thesis, we are going to mention and discuss the most studied variational DA methods namely; three Dimensional Variational data assimilation (3D-Var) and four Dimensional Variational data assimilation (4D-Var).

2.3.1 3D-Var assimilation

The idea behind 3D-Var is to find the optimal model state $\hat{\xi}$ that minimizes a (scalar) cost function $J(\xi)$ as given in Lorenc (1986, 1997), which measures the total distance between the model state and the background ξ_b and between the model state and the observation Υ.

$$J(\xi) = \frac{1}{2}(\xi - \xi_b)^T C_{\varepsilon^p}^{-1}(\xi - \xi_b) + \frac{1}{2}(\Upsilon - \mathscr{K}(\xi))^T C_{\varepsilon^o}^{-1}(\Upsilon - \mathscr{K}(\xi)) \tag{2.29}$$

The relative weights to the cost function for the background term and observation term are defined with respect to the observation error covariance matrix C_{ε^o} and the prior error covariance matrix C_{ε^p}, respectively.

The analytical solution for the minimization of cost function (2.29) is very expensive for large scale problems, and therefore the use of numerical optimization methods make it feasible; for example quasi-Newton optimization schemes, which are well presented in literature (e.g in Bonnans et al. (2006); Nocedal and Wright (1999)). If both the evolution model and the observation operators are linear, then a minimum variance unbiased estimator for ξ here denoted by $\hat{\xi}$ minimizes cost function (2.29) (Simon, 2006). This is important because the covariance matrix of the estimate denoted

by $\hat{C}^k_{\varepsilon^p}$ is given by the inverse Hessian of (2.29). This technique is useful for numerical method optimization and can be extended to nonlinear cases as well.

The 3D-Var has been put to operational use in many weather centers around the world within the last two decades, for example, the United Kingdom Meteorological Office (UKMO) had developed it in 1995 (Lorenc, 1997) and put operational use in 1999 (Lorenc et al., 2000). At the European Centers for Medium-Range Weather Forecasts (ECMWF), the method has become operational along with the more advanced 4D-Var scheme in 1996 (Courtier et al., 1998). Also, at Canadian Meteorological Centre (CMC) in 1997 (Gauthier et al., 1999). It has been reported, in all these centers that there was a significant improvement of the analysis compared to their previous methods; the nudging method for UKMO (Rawlins et al., 2007), statistical interpolation methods for CMC (Gauthier et al., 1999) and optimal interpolation for ECMWF (Andersson et al., 1998).

2.3.2 4D-Var assimilation

It has been a major ambition for meteorologists to have better forecasts, the use of measurements over a period of time as opposed to 3D-Var which uses measurements at analysis time only. The 4D-Var method is an extension of the 3D-Var method, with the addition of time dimension as the fourth dimension. The quality of the forecast has been significantly improved, with extension made using the 3D-Var code and the model code to make a 4D-Var scheme with minimal change in the code (Lorenc and Rawlins, 2005; Gauthier et al., 2007). The cost function for the 4D-Var is defined by Equation (2.30). Other versions of the cost functions (2.29) and (2.30) that use an incremental approach can be referred to example in Li et al. (2008) and Gauthier et al. (1994), respectively.

$$J(\xi) = \frac{1}{2}(\xi - \xi_b)^T C^{-1}_{\varepsilon^p}(\xi - \xi_b) + \frac{1}{2}\sum_{r=1}^{R}(\Upsilon_r - \mathscr{K}_r(\xi_r))^T C^{-1}_{\varepsilon^o}(\Upsilon_r - \mathscr{K}_r(\xi_r)) \tag{2.30}$$

where $r = 1, 2, ..., R$ are the time points of measurements and the model state at time point r (ξ_r) is given by the model evolution from time t_1 to time t_r by $\xi_r = \mathscr{M}(\xi_b)$. One advantage of the 4D-Var is that, it trains the model behavior in a period of time back and forth. This is contrary to the 3D-Var which learns only from the background. In this formulation, we can clearly see that the optimization of the cost function (2.30) is constrained. Apart from being theoretically attractive, 4D-Var had been computationally expensive. That lead to a number of studies to make it operationally possible (e.g see Gauthier et al. (1994)). Naturally, the background term can be easily computed, the burden of the 4D-Var comes firstly from the observation term that requires R model integrations. Secondly the gradient of the cost function (2.30) is hard to compute, and the use of the adjoint technique must be applied (Le Dimet and Talagrand, 1986). Nonetheless, it is worth putting a huge effort to build the adjoint code, because once it is made it can be used in a number of applications.

4D-Var has been an operational DA scheme in many weather centers around the world; at ECMWF since 1997 (Klinker et al., 2000), UKMO since 2004 (Lorenc and Rawlins, 2005; Rawlins et al., 2007) and at CMC implemented in 2005 (Gauthier et al., 2007), that reported positive improvement to the 3D-Var method forecast.

2.4 Hybrid methods

It has been shown earlier that ensemble methods have two attractive features; the forecast statistics produced are of good quality and can be even cheaper to obtain by just running the ensemble members in parallel. This has been also supported by several studies (e.g see in Kauranne (1992); Hamill

and Snyder (2000); Lorenc (2003)), that ensemble's covariance information should be used in the variational context to improve the analysis. Affordability for attaining high quality background statistics from ensemble methods is constrained with the requirement of a large number of ensemble members, which are not desired in computations, especially for large-scale high dimensional models. On the other hand, we have seen how good quality analysis produced by the variational method by weighing statistics between observation and background covariance. These two properties make an interesting topic of combining the two methods, to get so called hybrid method, which have had a limited number of studies so far. One can refer to some of the studies given here (Hamill et al., 2000; Hamill and Snyder, 2000; Hunt et al., 2007; Fertig et al., 2007; Wang et al., 2008) and more recently in Clayton et al. (2013); Lorenc et al. (2015).

The state of the art of hybrid methods slightly differ from one another. Kauranne (1992) suggested a coupling of EnKF and 4D-Var rather than hybriding, but the idea is still the same, to use ensemble forecasts to obtain full resolution 4D variational analyses over a long assimilation period. This will provide full resolution initial perturbations calculated daily from the operational dynamic model (Kauranne, 1992). In Hamill and Snyder (2000), an EnKF and 3D-Var hybrid method was developed, where the background error covariance was obtained as a linear combination from the time independent 3D-Var background covariance and time dependent background covariance from the EnKF with perturbed observations, whose noise matches to that of observations. This version of the hybrid method is a revised version of a similar method by Hamill et al. (2000), which does not utilize the background propagation statistics over time in 3D-Var analysis. A similar hybrid DA method that uses a 4D-Var cost function instead is presented in Fertig et al. (2007). The choice of the linear combination parameter is something that needs to be carefully studied in this approach, which might be used as an advantage to provide more weight to 3D-Var background covariance than EnKF covariance, if we are limited to low ensemble sizes. In Wang et al. (2008), the formulation of an Ensemble Transform Kalman Filter (ETKF) 3D-Var data assimilation (ETKF-3DVAR), is close to the one presented in Hamill and Snyder (2000), the exception is that the latter uses ETKF in getting time dependent covariance information. To guarantee total background error variance preservation, both formulations in Hamill and Snyder (2000) and Wang et al. (2008) impose a constraint (2.31) on the linear combination parameters for the error covariance from static (3D-Var) and dynamic (Ensemble method) component, the equation is

$$\frac{1}{a_1} + \frac{1}{a_2} = 1 \tag{2.31}$$

where a_1 and a_2 are linear combination parameters for the static background covariance and the flow dependent covariance respectively. Other hybrid methods developed at UKMO by Clayton et al. (2013), use ETKF and 4D-Var in its assimilation, employing a similar trick of linear combinations described in Hamill and Snyder (2000); Wang et al. (2008).

The results in the three cases of Hamill and Snyder (2000); Wang et al. (2008); Clayton et al. (2013), prove that the use of hybrid methods give superior result compared to separate methods; either EnKF alone or 3D-Var alone or 4D-Var alone. In Wang et al. (2008), the results for ETKF-3DVAR, applied in the north America region with the Weather Research Forecast (WRF) model to assimilate wind and temperature observations gives 15% and 20% improvement over 3D-Var. The results reported in Clayton et al. (2013) gave less than 1% average reduction in root mean square error (RMSE). This implies that is not worth adding high computation cost with that gain, but worth studying for better algorithms to improve the quality of the analysis. The good thing for this method is that it has

been implemented operationally since July 2011 by the UKMO for more studies and tests (Clayton et al., 2013).

The methods presented here do not account for the model error, which can easily introduce wrong background covariance information from the ensemble. Due to the fact that models always contain an error, this can be a serious blow for low ensemble size cases.

2.5 Fields of application

Data assimilation has been widely applied in the fields of meteorology, oceanography and hydrology. There is growing attention in other fields of science and engineering to accommodate DA. Data assimilation has been commonly used in two kinds of problems. The first one is to estimate the model state and hence compute a forecast. This is commonly applied in the field of meteorology, oceanography and hydrology (see for example in Barker et al. (2004); Li et al. (2008); Amour et al. (2013)). In Amour et al. (2013), the flow of a water wave in a dam-break experiment is assimilated using a hybrid DA method. While in Barker et al. (2004), a typhoon bogusing case has been studied using the 3D-Var method supported by a single surface pressure observation. In both cases of Barker et al. (2004) and Amour et al. (2013) the results were reported to be improved over that of pure simulations. The work of Li et al. (2008) presents a theoretical 3D-Var DA method for regional ocean modeling, in which case the formulation and error analysis are clearly presented.

The second application is on model parameter estimation. The DA procedure is used to estimate the parameters of the model using measurement data as the training set (Moradkhani et al., 2005; Kondrashov et al., 2008; Smith et al., 2013; Ruiz and Pulido, 2015). In Moradkhani et al. (2005) and Kondrashov et al. (2008), EnKF and EKF, respectively have been used to estimate both model state and model parameters. It has also been found that the model forecast is improved when the parameter are estimated (Kondrashov et al., 2008). It has been shown in Ruiz and Pulido (2015) how EnKF has been used to estimate both the parameter and the model state. The results of the assimilation have been accordingly improved for the imperfect atmospheric general circulation model used in the assimilation. For the case of 3D-Var, model state and parameter estimation have been studied with a 2D morphodynamic model of Morecambe Bay United kingdom by Smith et al. (2013). Again the results of the assimilation were encouraging. Another case where DA has been applied is on model error estimation (see for example in Zupanski and Zupanski (2006); Hamill and Whitaker (2005)). In Zupanski and Zupanski (2006), a method based on the hybrid DA method of Zupanski (2005) is proposed. The method provide estimates of the model state, model error and the uncertainties associated with them based on the analysis and forecast error covariance matrices.

Other fields in science are also following the trend in DA. The work of Zhang et al. (1999); Li et al. (2013); Mano et al. (2015) are good examples of DA studies related to environmental variables. A 3D-Var method has been used to assimilate the aerosol concentrations in Los Angeles basin in Li et al. (2013). In Zhang et al. (1999), the KF method has been applied to assimilate the level of methane gas CH_4 budget in the atmosphere of Europe with simulated and real CH_4 data. In the work of Mano et al. (2015), total suspended matter was assimilated using satellite images data in lake Säkylän Pyhäjärvi in South-West Finland. The results of these large-scale problem assimilations were reported to be substantial (Zhang et al., 1999; Mano et al., 2015), in (Li et al., 2013) with an improvement of forecast of aerosols for up to 24 hours. In the fight against global warming, the use of DA in environmental modelling might improve our understanding of environmental hazard variables. Therefore, appropriate actions and measures can be accordingly taken.

CHAPTER III

Variational Ensemble Kalman Filtering

The introduction of the Variational Ensemble Kalman Filter (VEnKF) by Solonen et al. (2012) is motivated by the fact that ensemble methods provide the nice feature of background error covariance propagation over time using a nonlinear model, while the variational methods offer a robust approach for determining an analysis relative to the background and observation covariances. Because background error covariance is propagated by the nonlinear model using the ensemble, we have avoided a cumbersome coding of tangent linear and adjoint codes for the model. This method is a close relative of Maximum Likelihood ensemble Filter (MLEF) introduced by Zupanski (2005), the difference being that MLEF does not account for model error and therefore is more susceptible to error growth and hence divergence.

3.1 Formulation of VEnKF

The VEnKF formulation has been inspired by the variational methods, in particular the Variational Kalman Filter (VKF) by Auvinen et al. (2010), which uses a numerical optimization algorithm to estimate the background error covariance, C_{ε^p} and uses the estimated covariance in a second optimization of the 3D-Var cost function (2.29) to get the analysis. As in the KF algorithm, the covariance is updated using the KF Equation (2.13), substituting this covariance into the subproblem (3.1)

$$\arg\min_u \frac{1}{2}\langle Au, u\rangle - \langle b, u\rangle \tag{3.1}$$

where $A = C_{\varepsilon^p} = \mathrm{M}_k \hat{C}_{\varepsilon^p}^{k-1} \mathrm{M}_k^T + C_\varepsilon^k$ and b is a zero vector. In the original version of Auvinen et al. (2010), the LBFGS algorithm (presented in section 3.1.1) was used to optimize (3.1). As a result, the inverse Hessian $C_{\varepsilon^p}^{-1}$, was obtained directly, ready to be used in the second LBFGS optimization with the 3D-Var cost function (2.29). The second optimization yields the state analysis and the estimate for the posterior, inverse Hessian of the estimate, $\hat{C}_{\varepsilon^p}^k$ that is needed in next assimilation cycle.

A nice feature in VKF is that, it avoids all matrix algebra complications demanded by the traditional KF. As a result VKF could be easily adapted in large-scale high dimensional models with low computational cost. The results for the VKF were comparatively very similar to the EKF in terms

of root mean square error of the forecast, tested with the toy Lorenz 95 model (Auvinen et al., 2010). A similar approach which employs variational methods and KF is developed in Auvinen et al. (2009), namely Large-Scale KF with the Limited Memory Broyden, Fletcher, Goldfarb and Shannon (BFGS) method (LBFGS-KF). The computational time for LBFGS-KF has been reduced by 10 times compared to that of KF (Auvinen et al., 2009). This feature suggests the method might suit well for large-scale problems.

3.1.1 LBFGS optimization: a subproblem in VEnKF

The Broyden-Fletcher-Goldfarb-Shanno (BFGS) algorithm is a quasi-Newton method known for its superlinear convergence (Nocedal and Wright, 1999; Bonnans et al., 2006). It is named after those scientists who contributed to its discovery.

The materials of the algorithm presented here are extracted from the literature (Nocedal and Wright, 1999; Bonnans et al., 2006). The function $f(x)$ to be minimized is approximated with the quadratic model at the current iterate x_k as follows:

$$m_k(p) = f_k + \nabla f_k^T p + \frac{1}{2} p^T B_k p \tag{3.2}$$

where $f_k = f(x_k)$, $\nabla f_k = \nabla f(x_k)$ and B_k is an $n \times n$ symmetric positive definite Hessian matrix which will be updated at every iteration. The value of x_k is updates using

$$x_{k+1} = x_k + \alpha_k p_k \tag{3.3}$$

where $p_k = -B_k^{-1} \nabla f_k$ is the direction vector, α_k is the step length at iteration k, the choice of α_k will be based on the Wolfe conditions (3.4), c_1 and c_2 are real constants, whose values are $c_1 \in (0, 1)$ and $c_2 \in (c_1, 1)$. In practice c_1 is set very small, say $c_1 = 10^{-4}$ (Nocedal and Wright, 1999). Alternatively, the value of the line search parameter α_k can be computed using an exact line search method (see e.g in Nocedal and Wright (1999)).

$$f(x_k + \alpha_k p_k) \leq f(x_k) + c_1 \alpha_k \nabla f_k^T p_k \tag{3.4a}$$

$$\nabla f(x_k + \alpha_k p_k)^T p_k \geq c_2 \nabla f_k^T p_k \tag{3.4b}$$

The above formulae are similar to the line search Newton method but here an approximate Hessian B_k is used instead of the true Hessian. The approximate Hessian is updated using the formula

$$B_{k+1} = (\mathbf{I} - \rho_k y_k s_k^T) B_k (\mathbf{I} - \rho_k y_k s_k^T) + \rho_k y_k y_k^T \tag{3.5}$$

where

$$\rho_k = \frac{1}{y_k^T s_k}, \qquad s_k = x_{k+1} - x_k, \qquad y_k = \nabla f_{k+1} - \nabla f_k$$

The formula (3.5) is called the DFP (Davidon, Fletcher and Powell) updating formula. We can also obtain another update formula by imposing a condition on the inverse Hessian H_k, that is $H_k = B_k^{-1}$. The updated matrix H_{k+1} in Equation (3.6) is the BFGS update formula

$$H_{k+1} = (\mathbf{I} - \rho_k s_k y_k^T) H_k (\mathbf{I} - \rho_k s_k y_k^T) + \rho_k s_k s_k^T \tag{3.6}$$

For computational cost efficiency, a Limited memory BFGS (LBFGS) uses only the most recent m vectors (from m iterations) to approximate the Hessian matrix. At iteration k, the current iterate is x_k and the pairs is $\{s_i, y_i\}$ for $i = k-m, k-m+1, ..., k-1$. We choose the initial approximation H_k^0 which can vary from iteration to iteration. The H_k approximation is then found to satisfy Equation (3.7) (Nocedal and Wright, 1999). Setting $V_k = \mathbf{I} - \rho_k s_k y_k^T$ we see that

$$\begin{aligned} H_k =& \big(V_{k-1}^T \cdots V_{k-m}\big) H_k^0 \big(V_{k-m} \cdots V_{k-1}\big) \\ &+ \rho_{k-m} \big(V_{k-1}^T \cdots V_{k-m+1}^T\big) s_{k-m} s_{k-m}^T \big(V_{k-m+1} \cdots V_{k-1}\big) \\ &+ \rho_{k-m+1} \big(V_{k-1}^T \cdots V_{k-m+2}^T\big) s_{k-m+1} s_{k-m+1}^T \big(V_{k-m+2} \cdots V_{k-1}\big) \\ &+ \cdots \\ &+ \rho_{k-1} s_{k-1} s_{k-1}^T \end{aligned} \tag{3.7}$$

From the expansion (3.7), we can compute the product $H_k \nabla f_k$ needed to update x_k in Equation (3.3) efficiently without storing the full matrix H_k. The LBFGS algorithm is summarized in Algorithm 3.1. Within the first $(m-1)$ iterations, the algorithm of LBFGS and that of BFGS give the same result if we fix $H_k^0 = H_0$. For thorough details and different flavors of quasi-Newton methods including the LBFGS, one can refer to the following studies of Broyden (1970); Matthies and Strang (1979); Gilbert and Nocedal (1993); Wei et al. (2006); Xiao et al. (2008).

Algorithm 3.1 LBFGS

$k \longleftarrow 0$
repeat
  Choose H_k, appropriately
  Compute $p_k \longleftarrow -H_k \nabla f_k$ with the help of (3.7)
  Compute $x_{k+1} = x_k + \alpha_k p_k$, where α_k is chosen to satisfy Wolfe conditions
  if $k > m$ **then**
    Discard the vector pair $\{s_{k-1}, y_{k-1}\}$ from storage
  end if
  Compute and save $s_k \longleftarrow x_{k+1} - x_k, \quad y_k \longleftarrow \nabla f_{k+1} - \nabla f_k$
  $k \longleftarrow k+1$
until convergence

3.1.2 The VEnKF Algorithm

The starting point of VEnKF algorithm is the VKF algorithm. VEnKF can also be seen as a variational method which uses ensemble methods to estimate background covariance matrix. The model state is estimated by optimizing the 3D-Var cost function (2.29). The background error covariance is estimated from the ensembles, with the following statistics that assumes the model error and the background are independent

$$C_{\varepsilon^p}^k = \mathrm{cov}(\mathscr{M}_k(\xi_{k-1}) + \varepsilon) = \mathrm{cov}(\mathscr{M}_k(\xi_{k-1})) + \mathrm{cov}(\varepsilon) = \mathbf{X}_k \mathbf{X}_k^T + C_\varepsilon$$

where $\mathbf{X}$ is defined as

$$\mathbf{X}_k = \frac{1}{\sqrt{n}} (\hat{X}_{k,1} - \hat{\xi}_k)(\hat{X}_{k,2} - \hat{\xi}_k), \cdots, (\hat{X}_{k,n} - \hat{\xi}_k) \tag{3.8}$$

The inverse of $C_{\varepsilon^p}^k$ required by the cost function (2.29) can be obtained in a similar fashion as in VKF, with optimizing the subproblem (3.9)

$$\arg\min_u u^T\big(\mathbf{X}_k\mathbf{X}_k^T + C_\varepsilon\big)u \tag{3.9}$$

For computing efficiency, the covariance matrix in (3.9) does not need to be computed explicitly, but can be kept in ensemble form, thus allowing for easy matrix products. To achieve this, one can write (3.9) as

$$\arg\min_u \big(u^T\mathbf{X}_k\mathbf{X}_k^T u + u^T C_\varepsilon u\big)$$

The minimization of the subproblem (3.9) will give the inverse background covariance using the LBFGS optimization. As it appears in Solonen et al. (2012), the inverse background covariance matrix $C_{\varepsilon^p}^{-1}$, can also be computed using the Sherman-Morrison-Woodbury (SMW) matrix inversion formula, one can find it, e.g in Hager (1989); Arias et al. (2015).

$$\begin{aligned} {C_{\varepsilon^p}^k}^{-1} &= (\mathbf{X}_k\mathbf{X}_k^T + C_\varepsilon)^{-1} \\ &= C_\varepsilon^{-1} - C_\varepsilon^{-1}\mathbf{X}_k(\mathbf{I} + \mathbf{X}_k^T C_\varepsilon^{-1}\mathbf{X}_k)^{-1}\mathbf{X}_k^T C_\varepsilon^{-1} \end{aligned} \tag{3.10}$$

Again this expression can be inserted directly into the cost function (2.29) without explicit evaluation. The computation is done in such a way that the matrix products are handled by nesting the matrix vector products in (2.29). The inverse of $(\mathbf{I} + \mathbf{X}_k^T C_\varepsilon^{-1}\mathbf{X}_k)$ has to be computed once if we assume constant model error (Solonen et al., 2012). Whose size is $n \times n$, which is advantageous for large scale problems. We thereby avoid inverting a covariance matrix whose size is determined by the size of model state vector. This problem is similar to transforming a problem from model state space to ensemble space.

With the use of LBFGS in minimization of the cost function (2.29), we obtain the model state analysis $\hat{\xi}_k$ and the low-storage estimates for the covariance matrix $\hat{C}_{\varepsilon^p}^k$, where a new ensemble is sampled from a normal distribution with mean $\hat{\xi}_k$ and covariance $\hat{C}_{\varepsilon^p}^k$.

$$X_{k,i} \sim \mathbf{N}(\hat{\xi}_k, \hat{C}_{\varepsilon^p}^k), \;\; i = 1, 2, \cdots, n$$

In the sampling procedure one can approximate the inverse Hessian of (2.29) by using either full rank low-memory representation obtained by the LBFGS unconstrained optimizer (Nocedal and Wright, 1999) or the reduced rank representation in the Krylov space created by conjugate gradient minimization of cost function (2.29) (Bardsley et al., 2013). Assume the inverse Hessian matrix H_k can be decomposed into the form $H_k^0 = L_0 L_0^T$, then as in Solonen et al. (2012), the sampling procedure is achieved with minimal effort by writing (3.7) into

$$H_k = Q_0 Q_0^T + \sum_{i=1}^{m} q_i q_i^T$$

where

$$\begin{aligned} Q_0 &= \big(V_{k-1}^T \ldots V_{k-m}^T\big)L_0 \\ q_1 &= \sqrt{\rho_{k-1}}s_{k-1} \\ q_i &= \sqrt{\rho_{k-i}}\big(V_{k-1}^T \ldots V_{k-i+1}^T\big)s_{k-1}, \ldots i = 2, \ldots m \quad \text{and } \rho_i > 0 \;\; \forall i \end{aligned}$$

Q_0 is a $N \times N$ matrix, N is the dimension of the model state vector and q_i are vectors of size $N \times 1$. Using the above representation, one can draw a vector r with zero mean $r \sim \mathbf{N}(\mathbf{0}, H_k)$ with the help of

$$r = Q_0 z + \sum_{i=1}^{m} \omega_i q_i \tag{3.11}$$

where $z \sim \mathbf{N}(\mathbf{0}, \mathbf{I})$ and $w \sim \mathbf{N}(0, 1)$. Again the matrix product $B_0 z$ can be nested with the stored LBFGS vectors for computational efficiency. As presented in Solonen et al. (2012), the VEnKF algorithm is summarized in Algorithm 3.2.

Algorithm 3.2 VEnKF

0. Initialization
   Initialize $\hat{\xi}_0$ and $X_{i,0}$, $i = 1, 2, \cdots, n$
   $k \leftarrow 1$
1. Propagation
   Propagate the background $\xi_k = \mathscr{M}(\hat{\xi}_{k-1})$
   Propagate the ensemble $\hat{X}_{k,i} = \mathscr{M}(X_{i,k-1})$, $i = 1, 2, \cdots, n$
2. Subproblem
   Get ${C_{\varepsilon^p}^k}^{-1}$ by using SMW (3.10) or LBFGS minimization to (3.9)
3. Assimilation
   Apply LBFGS in (2.29) to get $\hat{\xi}_k$ and $\hat{C}_{\varepsilon^p}^k$
   Generate new ensembles $X_{k,i} \sim \mathbf{N}(\hat{\xi}_k, \hat{C}_{\varepsilon^p}^k)$, $i = 1, 2, \cdots, n$

VEnKF differs from EnKF in many aspects. One particular difference is that in VEnKF the dynamic model is assumed imperfect which improves the chance of ensemble members to capture the covariance of the state by incorporating the model error into the dynamics. Also, the state analysis is the mode as opposed to basic EnKF in which it is the statistical mean of the ensemble. New ensemble members in VEnKF are generated every time the assimilation is performed, which is different to EnKF in which they are created at the beginning and propagated all over the assimilation time, which may cause filter inbreeding problems. As in all other ensemble methods, VEnKF can be easily implemented to run in a parallel environment for cheaper running cost and fast computation. These properties make the VEnKF a good candidate for large-scale problems using affordable means of computation.

3.2 VEnKF test applications

3.2.1 Test case I: Lorenz 95 model

The basic rule of starting with simple and then proceed to complex applications applies to many novel DA methods. They are first tested with a simple but chaotic model. Lorenz 95 (L95), introduced by Lorenz (1996) is often used to serve this purpose. L95 is a chaotic model and it is difficult to predict its flow behavior and therefore it is suitable for testing the performance of new DA methods small-scale problems. The L95 has been designed in such a way that it mimics weather dynamics. It has linear, quadratic and constant terms for advection, dissipation, and external forcing

representations, respectively (Lorenz and Emanuel, 1998). The L95 system is defined by a set of Equations (3.12)

$$\frac{dx_i}{dt} = (x_{i+1} - x_{i-2})x_{i-1} - x_i + F, \;\; i = 1, 2, \ldots, 40 \tag{3.12}$$

where F is a forcing constant that prevents the total energy from reducing to zero. Cyclic boundary conditions have been set such that $x_{-1} = x_{39}$, $x_0 = x_{40}$ and $x_{41} = x_1$ (Lorenz and Emanuel, 1998).

In the VEnKF test, we chose 24 observation sites out of 40 model states, thus the observation operator K is defined in a similar way as in Amour (2008) and Auvinen et al. (2010)

$$[\mathrm{K}]_{rp} = \begin{cases} 1, & (r,p) \in \{(3j+i, 5j+i+2) | i = 1,2,3 \;\; j = 0,1,\ldots,7\} \\ 0, & \text{elsewhere} \end{cases}$$

Measurement data was obtained from the solution of the L95 model, by adding normally distributed noise with mean zero and covariance $(0.15\sigma_{\text{clim}})^2\mathbf{I}$, where $\sigma_{\text{clim}} = 3.641$ is known as the climatological simulation standard deviation for long simulations. The model error was set to be $C_\varepsilon = (0.05\sigma_{\text{clim}})^2\mathbf{I}$, and the observation error covariance was set to be $C_{\varepsilon^o} = (0.15\sigma_{\text{clim}})^2\mathbf{I}$. The initialization for both $\hat{\xi}_0$ and $\hat{C}^0_{\varepsilon^p}$ was 1 and $\mathbf{I}$ respectively.

Different ensemble sizes have been run to test the performance of the VEnKF and compared to the EnKF and EKF. Figure 3.1 demonstrates the root mean square error (RMSE) estimates for ensemble sizes of 10 members, the RMSE is defined by the Equation (3.13)

$$[\text{RMSE}]_k = \sqrt{\frac{||\hat{\xi}_k - \xi_k^{\text{true}}||^2}{d}} \tag{3.13}$$

where ξ_k^{true} is the true values obtained in model solution at time point k, that is used to generate artificial data. To illustrate the RMSE behavior, we plot a Figure 3.2 to compare RMSE from VEnKF with that from EKF and EnKF. Both VEnKF and EnKF demonstrate comparable results for larger ensemble sizes, but for lower ensemble sizes, the EnKF performed poorly. Similar tendency is shown by forecast skill plots presented in Figures 3.3 and 3.4.

3.2.2 Test case II: 2D Heat Equation

To experiment the properties of the VEnKF with the higher linear dimensional evolution model, we use the two-dimensional heat equation for this purpose. The heat equation is adapted in similar way as in Auvinen et al. (2010) and is given by the partial differential equation (PDE) (3.14)

$$\frac{\partial T}{\partial t} = \frac{\partial^2 T}{\partial x^2} + \frac{\partial^2 T}{\partial y^2} + \alpha \exp\left(- \frac{(x - 2/9)^2 + (y - 2/9)^2}{\sigma^2} \right) \tag{3.14}$$

where T is the temperature at coordinates x and y defined over the domain $\Omega = \{(x,y) | x, y \in [0,1]\}$, $\alpha \geq 0$ is a parameter that controls the heat source. The model has been discretized with a uniform $S \times S$ grid, which results in a linear forward model $\xi_{k+1} = \mathrm{M}\xi_k + f$, where M is the heat diffusion and f is a constant vector for the external forcing in PDE (3.14). The description in full can be referred in Auvinen et al. (2009, 2010) and Solonen et al. (2012). The state vector, which contains temperature fields in this application, can be adjusted with the grid size S. The observation

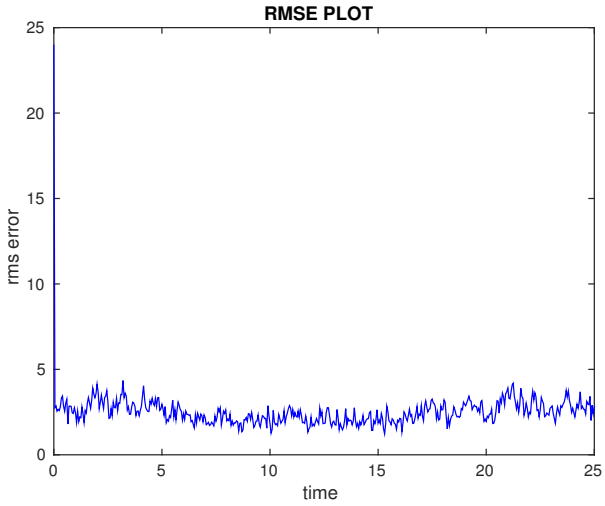

Figure 3.1: RMSE plot for the L95 model, the error decreases asymptotically and converges.

operator K is fixed over time as in Auvinen et al. (2010), where K is a full matrix with the following grid representations

$$\frac{1}{16}\begin{bmatrix}1 & 2 & 1\\ 2 & 4 & 2\\ 1 & 2 & 1\end{bmatrix}$$

The observation operator K maps the measured temperature array with grid lines equally spaced with $S^2/64$. Artificial data has been obtained by adding normally distributed noise to the model solution with the following representations

$$\xi_{k+1} = \mathrm{M}\xi_k + f + \mathbf{N}(0, (0.5\sigma_{ev})^2\mathbf{I})$$
$$\Upsilon_{k+1} = \mathrm{K}\xi_{k+1} + \mathbf{N}(0, (0.8\sigma_{obs})^2\mathbf{I})$$

To generate data the value of $\alpha = 0.75$ was used and σ_{ev} and σ_{obs} such that signal to noise ratio at the initial conditions, given by $||\xi_0||^2/S^2\sigma_{ev}^2$ and $||\mathrm{K}\xi_0||^2/S^2\sigma_{obs}^2$, are both 50. The initial condition used for data generation is

$$[\xi_0]_{ij} = \exp\big(-(x_i - 1/2)^2 - (y_j - 1/2)^2\big)$$

where x_i and y_j are the ith and jth grid point respectively. The value of $\alpha = 0$ is used for biased model setup, the model covariance error $C_\varepsilon = \sigma_{ev}^2\mathbf{I}$ and observation covariance error $C_{\varepsilon^0} = \sigma_{obs}^2\mathbf{I}$, the VEnKF algorithm uses the following update rules

$$\xi_{k+1} = \mathrm{M}\xi_k + \mathbf{N}(0, \sigma_{ev}^2\mathbf{I})$$
$$\Upsilon_{k+1} = \mathrm{K}\xi_{k+1} + \mathbf{N}(0, \sigma_{obs}^2\mathbf{I})$$

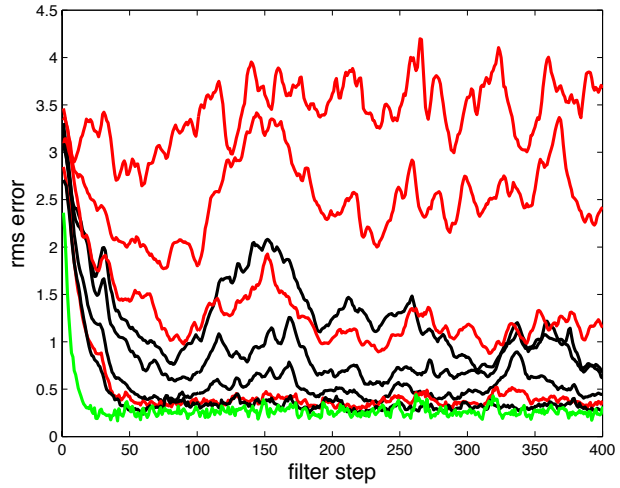

Figure 3.2: The L95 RMSE plot for VEnKF black curves, EnKF red curves and green curve for EKF. The ensemble sizes are 10, 15, 20 and 40 (Solonen et al., 2012).

First we set the model grid size of 32×32 and therefore model state vector was $S^2 = 1024$. We then compared the results of VEnKF with those of KF and EnKF using ensemble sizes of $n = 5, 10, 20, 50, 100$. In the optimization task, we used 20 LBFGS iterations and 20 stored vectors. The VEnKF results were approximately equal to the results of the KF with increasing ensemble sizes, but EnKF was not doing good with small ensemble sizes as shown in Figure 3.5.

A Second test was performed by increasing model grid resolution to 64×64, with the model state vector size $64^2 = 16384$. In this setup KF could not be used in our memory limited computational platform. The optimization parameters were kept the same as previous. The difference in performance between VEnKF and EnKF in this setup is more obvious, where VEnKF results were close to the 3D-Var with a fixed background error covariance results, as is visible in Figure 3.6.

3.3 Remarks

VEnKF has the unique feature of resampling on every analysis time step in contrast to the basic EnKF and its variants. This frequent resampling has the advantage of updating covariance error estimates from the analysis, and therefore keeping the filter away from inbreeding problems. The basic EnKF has often been criticized for adding additional sampling error caused by perturbed observations (Whitaker and Hamill, 2002; Zhang et al., 2009b; Acton, 2012). To alleviate the effect of perturbed observations, some new variants have been introduced, such as the square root EnKF (Tippett et al., 2003; Evensen, 2004; Acton, 2012; Nerger et al., 2012) and the Ensemble Transform Kalman Filter (ETKF) in Bishop et al. (2001); Nerger et al. (2012). As mentioned in Tippett et al. (2003), the square root filters suffer similar problem with basic EnKF with perturbed observations.

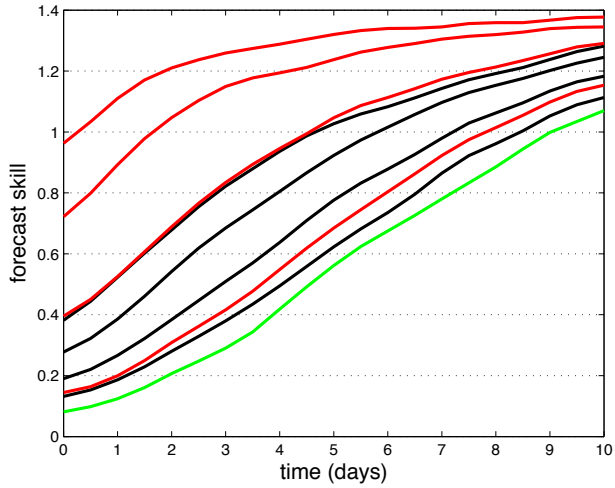

Figure 3.3: The L95 forecast skill plot for VEnKF black curves, EnKF red curves and green curve for EKF. The ensemble sizes are 10, 15, 20 and 40 (Solonen et al., 2012).

These ensemble methods has assume a perfect model, which sometimes cause them to underestimate error covariance and even filter divergence. To resolve the perfect model assumption, some adjustments have to be done, for example covariance inflation. In the VEnKF all these defects have been considered and are included in the minimization algorithm. Both model error and observation error are explicitly included in the cost function to be minimized. The square root filter works similar to the basic EnKF, by explicitly staying in the subspace spanned by the ensemble members, while VEnKF samples from the full state space (Solonen et al., 2012).

Methods related to VEnKF have been introduced in Hamill and Snyder (2000); Etherton and Bishop (2004); Wang et al. (2008). These are hybrid methods that combine 3D-VAR with basic EnKF with perfect model and perturbed observations. The prior covariance is assumed to be a linear combination of the sample covariance and the constant model error covariance defined in 3D-VAR. In the same way, Zhang et al. (2009a) presented hybrid methods that use ensemble methods with 4D-VAR, however the model error is still not incorporated into the assimilation, and thus does not address the drawback of model error exclusion.

The performance of VEnKF has been numerically shown to be better than the basic EnKF in the sense of RMSE estimates. Due to the use of the LBFGS method in the optimization and sampling, VEnKF has solved the same memory issue addressed in the KF (see Zhang et al. (1999); Evensen (2009) for example) and VKF methods. But, fine tuning of LBFGS parameters must be assured to obtain a stable filter. The good point for ensemble methods is that they can be easily run in parallel. This applies to VEnKF, too. This is a nice feature for the method to be useful in large-scale model assimilation. Lastly, but not least, VEnKF does need neither tangent nor adjoint codes, which are needed in the case of EKF and VKF implementation. These codes are cumbersome to make for advanced dynamics models.

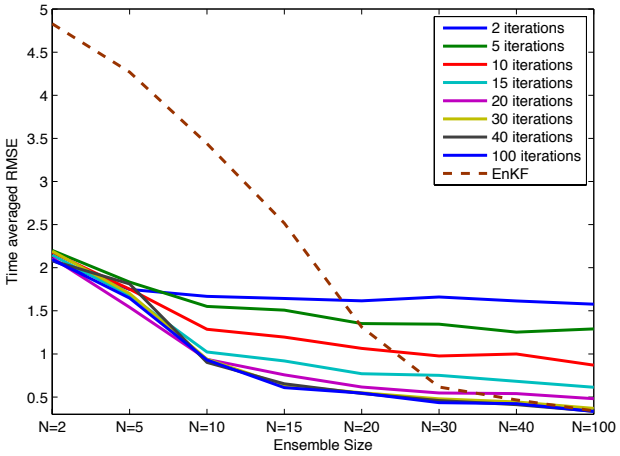

Figure 3.4: The L95 RMSE averaged over time plot for VEnKF and EnKF dashed curves, the ensemble sizes are shown on horizontal axis (Solonen et al., 2012).

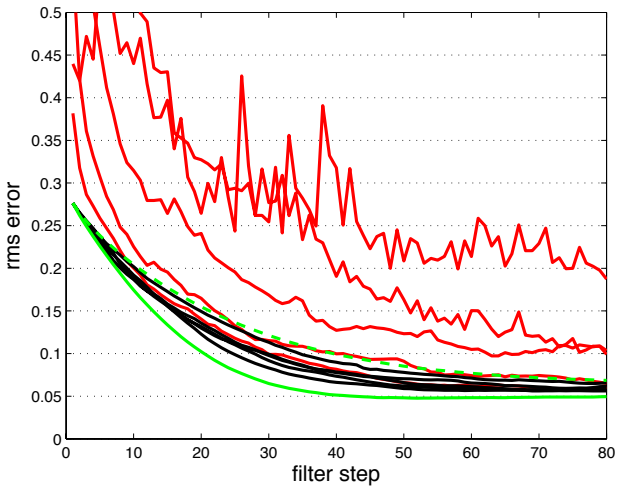

Figure 3.5: Comparison in performance between VEnKF (black), KF (solid green) and EnKF (red) with different ensemble sizes, where the grid size is 32×32. The dashed green line is 3D-Var where the model background error is fixed over time (Solonen et al., 2012).

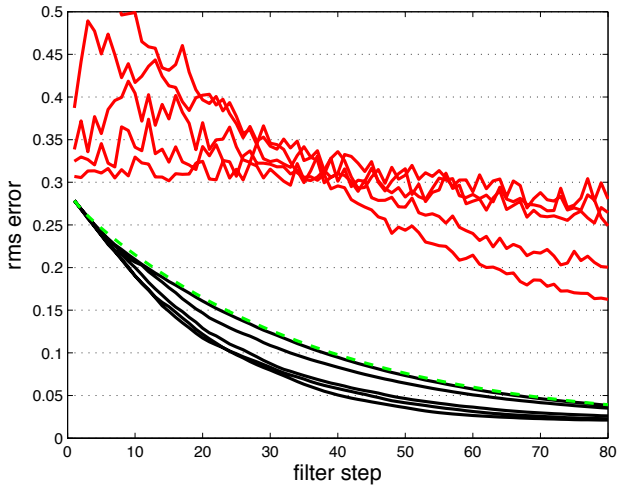

Figure 3.6: Comparison in performance between VEnKF (black) and EnKF (red) with different ensemble sizes, where the grid size is 64×64. The dashed green line is 3D-Var where the model background error is fixed over time (Solonen et al., 2012).

CHAPTER IV

VEnKF application to a dam-break experiment

4.1 Motivation

The results from the VEnKF method are promising and encouraging for more experiments to be carried out, since VEnKF has only been tested with small-scale and toy model problems, such as Lorenz 95 and 2D heat equation. Because performance of any assimilation method is judged by its robustness and accuracy in a variety of problems of different kinds and complexities. More advanced model dynamic problems would undoubtedly explore deeper the competence of the assimilation method in question.

One sources of complexity in model dynamics is turbulence. An experiment that is going to be presented here next exhibits turbulence. It is an extension of the work of Martin and Gorelick (2005), who studied a dam-break experiment of Bellos et al. (1991). The MATLAB source code for the model and simulation were made publicly available and goes with the name MOD_FreeSurf2D. The code implements semi-implicit, semi-Lagrangian time stepping algorithm of Casulli and Cheng (1992); Casulli (1999); Casulli and Zanolli (2002) and uses a finite volume discretization. Apart from being freely available, the other reason of selecting MOD_FreeSurf2D is the availability of all resources needed in assimilation including the measurements.

Pure 2D simulations of hydrodynamic flows are not perfect in practice. One reason is that the numerical flow is simplified to 2D, which can not capture the vertical flow, in particular when the flow is turbulent. More importantly, common numerical time stepping schemes imply that a flow front in front of a discontinuity, such as a flood wave, will only propagate one grid-line per time step (Amour et al., 2013). The speed of this shock wave is therefore dependent on grid size and the numerical time step, and not on the correct physical speed (Amour et al., 2013). With these arguments, there is no means to link the simulated flow to the true flow after the initial condition to be fixed. This can be achieved with the help of a DA procedure, and we are going to address all these defects.

4.2 Numerical simulation in hydrology

Complex geometry and meandering path of the river flows brings troubles to numerical computational schemes. Varieties of schemes have been adapted in many applications to best capture the

information of river hydrological flows, in some cases with minimal cost. In this manuscript we will mention some of these schemes and their areas of applications. A 2D finite-element method has been used to simulate 11 km long reach of River Culm in Devon, U.K., which has been modelled by 2D depth-averaged Reynolds equations (Bates and Anderson, 1993). The simulation results got an error of $\pm 2\%$ in continuity, however mass was fairly conserved. The same algorithm has been adapted to flow simulations in the work of Aliparast (2009). 2D shallow-water model equations were used, because of the influence of bottom roughness caused by turbulent shear stress between grids, the stress term is neglected (Yoon and Kang, 2004). An oblique hydraulic jump has been used to validate the model, where the analytical solution could be easily obtained (Aliparast, 2009). In other application, the scheme has been tested with a dam-break application in a converging-diverging flume (Bellos et al., 1991).

Another scheme which is popular in many computational fluid dynamics (CFD) numerical simulation is the finite volume method. It has been widely used in many applications, for example in shallow water models (Heniche et al., 2000; Zhang and Wu, 2011; Ying et al., 2009). A new approach on the dam-break case is demonstrated by Baghlani (2011), where a robust flux vector splitting (FVS) method is used. FVS has been applied to solving similar compressible flow problems frequently (eg. in (Baghlani, 2011; Erpicum et al., 2010; Toro and Vazquez-Cendon, 2012)). In this manuscript we will mention two FVS methods; that of Steger and Warming and that of Van Leer. Steger and Warming's FVS exploits the homogeneous characteristics of the Euler equation and splits the fluxes into positive and negative portions (Drikakis and Tsangaris, 1993). Van Leer's FVS creates fluxes that depend on the local Mach number (Drikakis and Tsangaris, 1993). The FSV proposed by Baghlani (2011) splits the flux vector into positive and negative parts by using a Jacobian matrix of flux vectors and a Liou-Steffan splitting for decomposing the pressure term. The FVS methods are very expensive in terms of computations, whereby the eigensystem of equations has to be computed at every time step (Baghlani, 2011).

One can also investigate hydrological flow behaviour by constructing flow properties directly from measurements. In Collischonn et al. (2005), an innovative part was that of using quantitative rainfall forecast and rainfall observations as data input to the river flow model for river Uruguay. The approach is very close to a DA procedure. The results were reported to be improved by using the input from the rainfall forecast and rainfall observation. A similar method of surface analysis and velocity changes of this type has been mentioned in Bárcena et al. (2012). The method uses regression of several model scenarios to generate a continuous function of hydrodynamic responses. The method has been successfully predicting velocity and estuarine free surface, with a very low computational cost for short and medium range simulation time. The obvious advantage for this method is its small computational times, but the model's phenomena are not guaranteed to be governed by the physical laws.

4.3 Depth Averaged Shallow Water Equations

The governing equations for MOD_FreeSurf2D are the depth-averaged shallow water equations. The MOD_FreeSurf2D equations are derived from simplified Navier-Stokes equations; comprising momentum Equations (4.1) and (4.2) and continuity Equation (4.3)

$$\frac{\partial u}{\partial t} + u\frac{\partial u}{\partial x} + v\frac{\partial u}{\partial y} + w\frac{\partial u}{\partial z} = -g\frac{\partial \eta}{\partial x} + \varepsilon\left(\frac{\partial^2 u}{\partial x^2} + \frac{\partial^2 u}{\partial y^2}\right) + \frac{\partial}{\partial z}\left(\nu\frac{\partial u}{\partial z}\right) + fv \tag{4.1}$$

$$\frac{\partial v}{\partial t} + u\frac{\partial v}{\partial x} + v\frac{\partial v}{\partial y} + w\frac{\partial v}{\partial z} = -g\frac{\partial \eta}{\partial y} + \varepsilon\left(\frac{\partial^2 v}{\partial x^2} + \frac{\partial^2 v}{\partial y^2}\right) + \frac{\partial}{\partial z}\left(\nu\frac{\partial v}{\partial z}\right) - fu \tag{4.2}$$

$$\frac{\partial u}{\partial x} + \frac{\partial v}{\partial y} + \frac{\partial w}{\partial z} = 0 \tag{4.3}$$

where $u(x, y, z, t)$, $v(x, y, z, t)$ and $w(x, y, z, t)$ are the directional velocity components in the horizontal x, y and z directions, t is the time variable, $\eta(x, y, t)$ is the water surface elevation measured from the undisturbed water surface, g is the gravitational constant, ε is the horizontal eddy viscosity, f is the Coriolis parameter and ν is the vertical eddy viscosity coefficient (Martin and Gorelick, 2005). Using the assumption of a well mixed water column with a shallow depth to width ratio, then one can integrate Equations (4.1)–(4.3) vertically.

$$U = \frac{1}{H}\int_{-h}^{\eta} u dz\ , \quad V = \frac{1}{H}\int_{-h}^{\eta} v dz$$

where U is the depth-averaged x-direction velocity component, V is the depth-averaged y-direction velocity component. Integration of continuity Equation (4.3) requires boundary conditions (4.4) and (4.5) at both the top and bottom of the water column respectively

$$\nu\frac{\partial u}{\partial z} = \gamma_T(U_a - U), \ \ \nu\frac{\partial v}{\partial z} = \gamma_T(V_a - V) \tag{4.4}$$

$$\nu\frac{\partial u}{\partial z} = g\frac{\sqrt{U^2 + V^2}}{C_z^2}U, \ \ \nu\frac{\partial v}{\partial z} = g\frac{\sqrt{U^2 + V^2}}{C_z^2}V \tag{4.5}$$

where γ_T is the wind stress coefficient, C_z is the Chezy coefficient, U_a and V_a are wind velocities. The integration of all Equations (4.1)–(4.3) provide the depth averaged shallow water equations (DASWE) (4.6) – (4.8)

$$\frac{\partial U}{\partial t} + U\frac{\partial U}{\partial x} + V\frac{\partial U}{\partial y} = -g\frac{\partial \eta}{\partial x} + \varepsilon\left(\frac{\partial^2 U}{\partial x^2} + \frac{\partial^2 U}{\partial y^2}\right) + \gamma_T\frac{(U_a - U)}{H} - g\frac{\sqrt{U^2 + V^2}}{C_z^2}U + fV \tag{4.6}$$

$$\frac{\partial V}{\partial t} + U\frac{\partial V}{\partial x} + V\frac{\partial V}{\partial y} = -g\frac{\partial \eta}{\partial y} + \varepsilon\left(\frac{\partial^2 V}{\partial x^2} + \frac{\partial^2 V}{\partial y^2}\right) + \gamma_T\frac{(V_a - V)}{H} - g\frac{\sqrt{U^2 + V^2}}{C_z^2}V - fU \tag{4.7}$$

$$\frac{\partial \eta}{\partial t} + \frac{\partial (HU)}{\partial x} + \frac{\partial (HV)}{\partial y} = 0 \tag{4.8}$$

where $H = h + \eta$ is the total water depth and h is the undisturbed water depth. Figure 4.1 illustrates the variable definitions of MOD_FreeSurf2D as in Martin and Gorelick (2005).

4.4 Numerical methods and boundary conditions

The discretization in MOD_FreeSurf2D is done using the Arakawa C-grid (Arakawa and Lamb, 1977) shown in Figure 4.2. In this representation, the evaluation of the horizontal components u and v are at the centres of the left and right grid faces and the centres of the lower and upper grid faces,

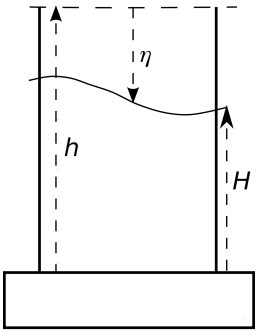

Figure 4.1: MOD_FreeSurf2D variable definition (side view) showing the relationship between free surface elevation η, total water depth H, and undisturbed water depth h.

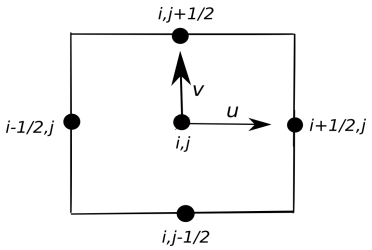

Figure 4.2: The Arakawa C-grid. All calculations of the vector components are performed at the centres of the edges of the grid faces.

respectively (Arakawa and Lamb, 1977). Semi-implicit, semi-Lagrangian time stepping scheme and a finite volume discretization has been employed together to numerically solve the shallow-water equations on a rectangular grid. The scheme assures a stable solution, even for a higher time step that exceeds Courant-Friedrichs-Levy (CFL) condition given by Equation (4.9)

$$\text{CFL} = w\frac{\Delta t}{\Delta x_i} \tag{4.9}$$

where w is the velocity component in x_i-direction, $i = 1, 2$, Δt is the time step size, and Δx_i is the cell dimension in the x_i-direction of flow (Martin and Gorelick, 2005). The CFL compares fluid velocity and time step size with computational grid size, and must be smaller than 1 for the scheme to be stable (Martin and Gorelick, 2005).

4.4.1 Semi-implicit scheme

In this case, the free surface elevation η and the horizontal velocity components U and V are the target variables to be found at time point $N+1$;

$$\begin{aligned}
\eta_{i,j}^{N+1} =& \eta_{i,j}^{N} - \theta\frac{\Delta t}{\Delta x}\left(H_{i+1/2,j}^{N}U_{i+1/2,j}^{N+1} - H_{i-1/2,j}^{N}U_{i-1/2,j}^{N+1}\right) \\
&- \theta\frac{\Delta t}{\Delta y}\left(H_{i,j+1/2}^{N}V_{i,j+1/2}^{N+1} - H_{i,j-1/2}^{N}V_{i,j-1/2}^{N+1}\right) \\
&- (1-\theta)\frac{\Delta t}{\Delta x}\left(H_{i+1/2,j}^{N}U_{i+1/2,j}^{N} - H_{i-1/2,j}^{N}U_{i-1/2,j}^{N}\right) \\
&- (1-\theta)\frac{\Delta t}{\Delta y}\left(H_{i,j+1/2}^{N}V_{i,j+1/2}^{N} - H_{i,j-1/2}^{N}V_{i,j-1/2}^{N}\right) \qquad (4.10)
\end{aligned}$$

$$\begin{aligned}
U_{i+1/2,j}^{N+1} =& FU_{i+1/2,j}^{N} - (1-\theta)\frac{g\Delta t}{\Delta x}\left(\eta_{i+1,j}^{N} - \eta_{i,j}^{N}\right) - \theta\frac{g\Delta t}{\Delta x}\left(\eta_{i+1,j}^{N+1} - \eta_{i,j}^{N+1}\right) \\
&+ \Delta t\frac{\gamma_T(U_a - U_{i+1/2,j}^{N+1})}{H_{i+1/2,j}^{N}} - g\Delta t\frac{\sqrt{(U_{i+1/2,j}^{N})^2 + (V_{i+1/2,j}^{N})^2}}{Cz_{i+1/2,j}^{2}H_{i+1/2,j}^{N}}U_{i+1/2,j}^{N+1} \qquad (4.11)
\end{aligned}$$

$$\begin{aligned}
V_{i,j+1/2}^{N+1} =& FV_{i,j+1/2}^{N} - (1-\theta)\frac{g\Delta t}{\Delta y}\left(\eta_{i,j+1}^{N} - \eta_{i,j}^{N}\right) - \theta\frac{g\Delta t}{\Delta y}\left(\eta_{i,j+1}^{N+1} - \eta_{i,j}^{N+1}\right) \\
&+ \Delta t\frac{\gamma_T(V_a - V_{i,j+1/2}^{N+1})}{H_{i,j+1/2}^{N}} - g\Delta t\frac{\sqrt{(U_{i,j+1/2}^{N})^2 + (V_{i,j+1/2}^{N})^2}}{Cz_{i,j+1/2}^{2}H_{i,j+1/2}^{N}}V_{i,j+1/2}^{N+1} \qquad (4.12)
\end{aligned}$$

where Δx is the computational grid size in the x-direction, Δy is the computational grid size in the y-direction, and Δt is the computational time step (Martin and Gorelick, 2005), where as $0.5 \leq \theta \leq 1$ adjusts the degree of implicitness of the solution. For $\theta = 0.5$ means the solution is centered in time and for $\theta = 1.0$ means the solution is completely implicit (Casulli and Cheng, 1992). The operators FU and FV in Equations (4.11) and (4.12) contain the advective, viscous, and coriolis components of the shallow water equations (Martin and Gorelick, 2005). The value of Chezy coefficient in Equation (4.13) is given in terms of Manning's roughness coefficient Mn, which is taken as dimensionless (Martin and Gorelick, 2005). More details of the discretization procedures can be referred in Martin and Gorelick (2005).

$$C_{z_{i+1/2,j}} = \frac{\left(H_{i+1/2,j}\right)^{1/6}}{Mn_{i+1/2,j}} \qquad (4.13)$$

4.4.2 The boundary conditions

The MOD_FreeSurf2D can determine the water/land location boundaries using the Equations (4.14) and (4.15) (Martin and Gorelick, 2005):

$$H_{i+1/2,j}^{N+1} = \max\left(0, h_{i+1/2,j} + \eta_{i,j}^{N+1}, h_{i+1/2,j} + \eta_{i+1,j}^{N+1}\right) \qquad (4.14)$$

$$H_{i,j+1/2}^{N+1} = \max\left(0, h_{i,j+1/2} + \eta_{i,j}^{N+1}, h_{i,j+1/2} + \eta_{i,j+1}^{N+1}\right) \qquad (4.15)$$

Two types of horizontal boundary conditions have been defined

i. The projection of the velocity normal to the domain boundary is imposed by Equation (4.16)

$$\frac{\partial U}{\partial t} + U_{upw}\frac{\partial U}{\partial n} = 0 \tag{4.16}$$

where U_{upw} is the up-winded normal direction velocity component, and n is the direction normal to the domain boundary (Martin and Gorelick, 2005).

ii. To control wave reflections at open boundaries, the Equation (4.17) imposes the condition

$$\frac{\partial \eta}{\partial t} + C_n\frac{\partial \eta}{\partial n} = 0 \tag{4.17}$$

where C_n is the propagation velocity from grid points around the boundary (Martin and Gorelick, 2005).

4.5 Experimental and VEnKF setups

The dam-break experiment consists of a 21.2 m long, 1.4 m wide flume. The flume is closed at one end and open at the other end. It has a curved constriction at a distance of 5.0 m from the closed end that ends at 4.7 m from the open end. A dam is placed at 8.5 m from the closed end with an opening 0.6 m wide. The flume is 0.002 steep with water at a height of 0.15 m behind the dam (Martin and Gorelick, 2005). Wave meters (marked with circles) and pressure transducers (marked with stars) were placed at 8 different locations, as shown in Figure 4.3, however the location number 7 did not record any measurement. The recorded water depths last for about a minute after the dam is broken. The dam position is set to be the origin, the wave meters are then assumes places $x = -8.5$, -4.5, and -0.0 m, and the pressure transducers placed at $x = +0.0$, $+2.5$, $+5.0$, $+7.5$, and $+10.0$ m (Martin and Gorelick, 2005). The computational time step used in the experiment is $\Delta t = 0.103$ s and the model grid sizes are $\Delta x = 0.05$ m and $\Delta y = 0.125$ m. The flume geometry is therefore sliced into 30×171 grid cells. The state vector ξ for the VEnKF assimilation is made of the arrays

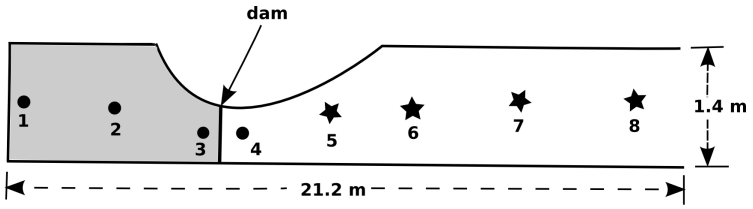

Figure 4.3: Unscaled plan view of the 21.2 m long 1.4 m wide flume.

of heights at the center of a grid point. In practice, the state vector has free surface elevation η, horizontal velocities U in the x-direction and V in the y-direction, i.e., $\xi = [\eta \ U \ V]^T$. The model has, therefore, altogether 16000 spatial degrees of freedom. The observation error and the model error covariance matrices are both assumed to be diagonal. The observation operator K is a linear operator that maps the state vector to the observation space corresponding to all grid points covered by the interpolated data, but restricted to the water height values only (Amour et al., 2013).

As evident from the cost function (2.29), the VEnKF does not account for additional prior knowledge beyond the observations and background. This is to say that in the case of bounded domains, one can not incorporate information about the boundaries into the filter analysis. If the evolution model automatically keeps the boundaries in order with given constraints, we can simply reduce the DA analysis to the inner part of the model domain. But, this approach is difficult when we have dynamic boundaries, which is not the case in the dam-break experiment presented here. The strategy that has been employed to achieve boundary constraints within VEnKF is that, we introduced the information of boundaries within the model error covariance C_ε. This changes the analytical representation of the boundaries to probabilistic representation. Because we know where the shore is located, we have defined the model error covariance with very small variances in the river bank area compared to the water flow area. This helps VEnKF to fairly respect the shore boundaries in DA analysis.

4.5.1 Experiment I: Artificial measurements

Again we employ a common practice in data assimilation to test the performance of the DA scheme with artificial experiments. One clear advantage from this is that the truth is known and therefore it is easy to evaluate the method with relevant statistical tools. The solution of the pure simulation has been contaminated with normally distributed with mean $\mathbf{0}$ and covariance of $0.05\mathbf{I}$ to make the data. To be realistic with the original setup of the dam-break experiment, data has been picked in all 8 places corresponding to wave meter locations defined in Martin and Gorelick (2005). Time interval between the data in all locations was fixed, but randomly chosen for every location. This setup mimics the fact that wave meters do not necessarily have measurement information at the same time.

Results: Figures 4.4 and 4.5 show the matching between the data, 50 ensemble members VEnKF estimates and the model simulation, here known as the truth, are displayed for all 8 meter locations. "The aim of this study is not really data assimilation for the purpose of a subsequent forecast with VEnKF, as would be the case in an atmospheric dynamics context, but instead qualitatively better hind-casting of a catastrophic event, such as a dam-breaking down, with an ensemble-based approach"(Amour et al., 2013). In this case, the period of a forecast is very short; just one computational time step. This close matching between the model and observations over one time step also results in very compact ensemble spreads, as it can be observed in Figure 4.6. RMSE in Figure 4.7 can tell us how much VEnKF estimates are from the true value, unfortunately can not tell us anything about the uncertainties of the estimates (Solonen et al., 2014).

4.5.2 Experiment II: Real measurements

In this experiment, we have used the published data set which has been used by Martin and Gorelick (2005) for comparison between pure simulation and the wave meter measurements. The data were too sparse for direct use in assimilation, which gave us no other option than to interpolate in time and space. Observations were coming at an average rate of 1.6 data in one or more locations per time step and at a maximum of 5 locations per time step. The data featured only measurements of water height. This is to say that the number of observations with respect to the dimension of state space is about $1/100000$, since the time step is 0.1 s. For this reason, the observations were interpolated in time by piecewise cubic Hermite Interpolating Polynomials (Fritsch and Carlson, 1980). Figure 4.8 shows the interpolated data together with the original height data. The data has also been

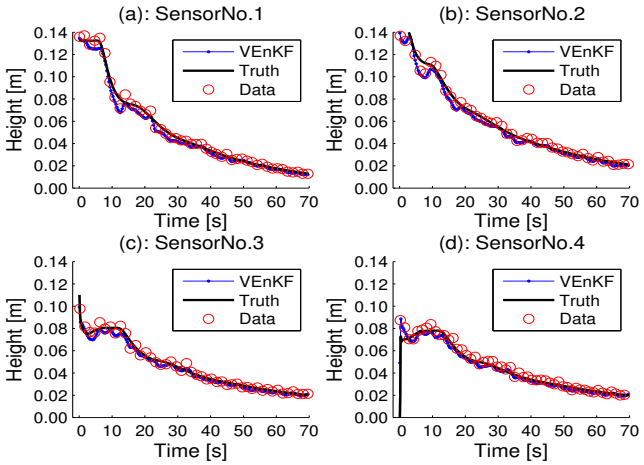

Figure 4.4: Data assimilation for artificially generated data for sensor locations 1 to 4 using 50 ensemble members. The blue line is the VEnKF, the red marks are the observations and the black trajectories are the truth (Amour et al., 2013).

interpolated in space by a Gaussian mask of 9×9 square patch, with decaying coefficients for the Gaussian kernel set to 0.2 and 0.05 along and across the flume respectively. These values have been chosen to ensure that it does not cause high fluctuations between the values in the neighborhoods. The idea is to make the data dense enough for the VEnKF assimilation scheme to be stable. That improved the ratio of the number of observations to state space dimension to $1/50$ as compared to $1/100000$ before interpolation.

The model error C_{ε}^{k} and the observation error covariance matrices $C_{\varepsilon^o}^{k}$ were set to $C_{\varepsilon}^{k} = (0.0011)^2\mathbf{I}$ and $C_{\varepsilon^o}^{k} = (0.001)^2\mathbf{I}$. The initial estimate of the state $\hat{\xi}$ was set to be equal to the height of water before the dam is broken and the initial covariance estimate $\hat{C}_{\xi^p}^{0} = \mathbf{I}$. The model is then run with 75 ensemble members, 25 LBFGS iterations and 25 LBFGS stored vectors.

Results: The results of the pure simulations with MOD_FreeSurf2D show that the simulated water depth matches well with the measured heights only for the first three upstream wave meters readings, see Figures 4.9(a)-(c). For the downstream locations, the results are less accurate due to the emergence of super-critical flows in the downstream end which is characterized by turbulent flow, because the model can tracks the height of water but not the turbulent fine structure of the flow. In Figure 4.9(d) as well as Figure 4.10(a) and (b) in particular, we can see the jumps of the flow at the beginning of the dam opening. Water depth variations with time is compared with interpolated data as shown for the seven sensors in Figures 4.11 and 4.12. It is clearly seen from the results that the location immediately after the dam (location 4) had defects in its flow nature, while VEnKF is able to approximate the water height and the structure of the flow. Similar situation observed in locations 5, 6 and 8, where the VEnKF captured fairly good the most visible features of the water flow. The VEnKF has shown it capabilities of capturing the flow behavior for all censors along the flume, this is different to the open loop simulation. This demonstrates the power of VEnKF in

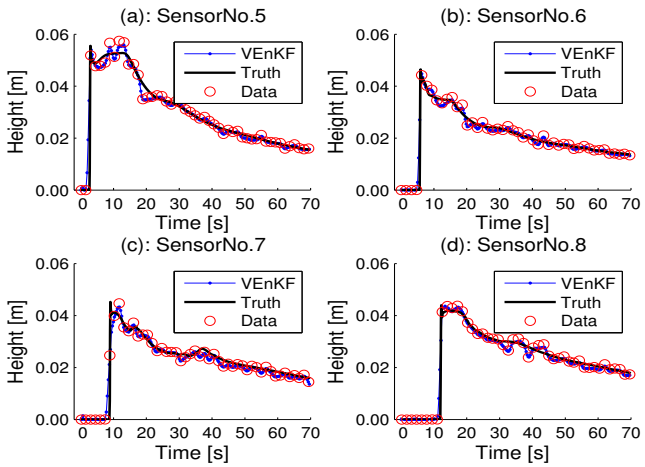

Figure 4.5: Data assimilation for artificially generated data for sensor locations 5 to 8 using 50 ensemble members. The blue line is the VEnKF, the red marks are the observations and the black trajectories are the truth (Amour et al., 2013).

predicting dam-break flows for river and streams. It is worth mentioning the time series of water depth at sensor location 7 that did not have any measurements. Comparing the pure simulated curve in Figure 4.10(c) to that of Figure 4.12(c) with VEnKF, one can agree that the latter contains similar fine scale oscillations due to small waves as the sensors with observations, these oscillations were missing in pure simulation in Figure 4.10(c). This is good behavior of DA procedure, it can give a realistic representation of other observation sites as well, even though did not have measured data.

4.6 Remarks

There is a growing trend of incorporating mathematical models with observational data in the field science and computing. Computer capacity has been making rapid progress in recent years. Innovation of different kind of automatic stations for data measurements improve the availability of reliable data for assimilation. DA methods are criticized as resources hungry in terms of computational and data availability, but with the above mentioned facts, DA is a phenomenon that is growing fast and is affordable.

In the assimilation of the dam-break experiment, we have shown how DA can bring advantages to hydrological simulations. The VEnKF results of the dam-break simulation behaves more naturally than the pure simulation alone. The turbulent behavior of water could not been realized but in VEnKF assimilation. The real flow, with turbulent characteristics which shows hydraulic jumps and avoids many numerical artifacts, like the one shown in Figure 4.10 is well reproduced by the VEnKF.

Another advantage from DA is a proper statistical treatment of flume simulations. Traditional mathematical models are deterministic whereas in pure simulation we can only approximate a real phys-

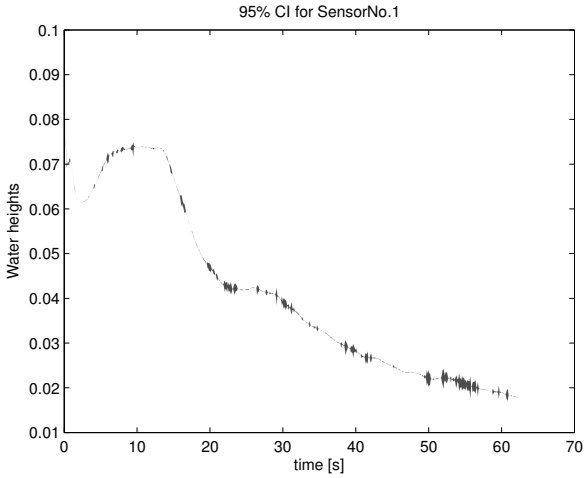

Figure 4.6: Very compact 95% confidence range is shown for the location of wave meter No. 1 (Amour et al., 2013).

ical phenomenon in a statistical sense. Therefore, the use of a version of Kalman filtering, the VEnKF, adds significant value to the simulation as it consistently incorporates information outside the physical model. The expected error covariance matrix of the analysis is well approximated in the course of DA.

Continuous DA consistently addresses qualitative defects in flow simulations and correctly interprets simulated numerical values as samples from a distribution of possible physical values, not as true physical values (Amour et al., 2013). One drawback for almost all DA methods is that, they do not respect the physical law of the model and therefore mass conservation should be separately studied and implemented. For the case of VEnKF, the mass conservative version has been studied and introduced in Seif (2015).

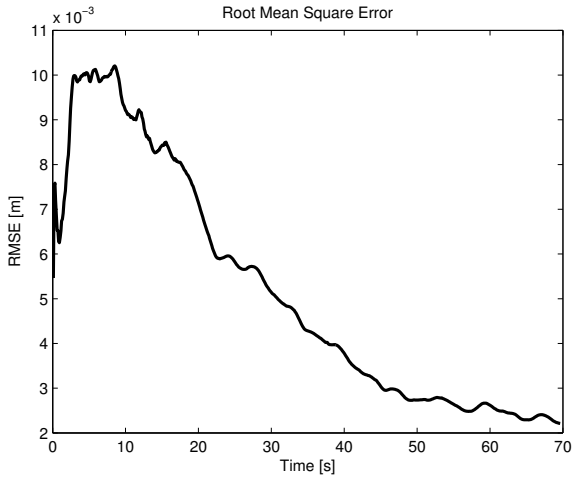

Figure 4.7: RMSE plot for the artificial experiment, the error reduced asymptotically (Amour et al., 2013).

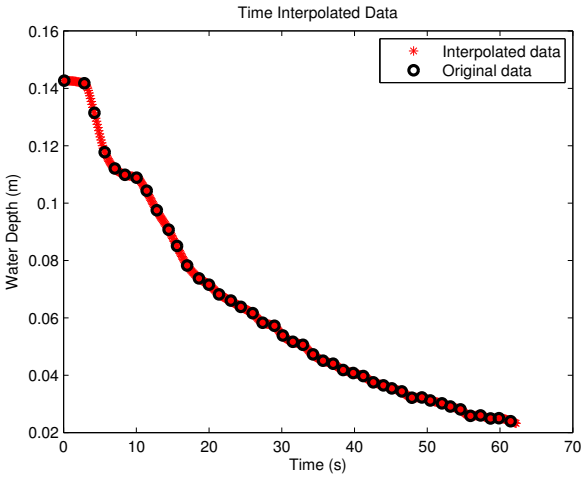

Figure 4.8: Time interpolation of water heights at sensor location 2, to cover the whole period of simulation with interpolated data at an interval corresponding to one computational time step.

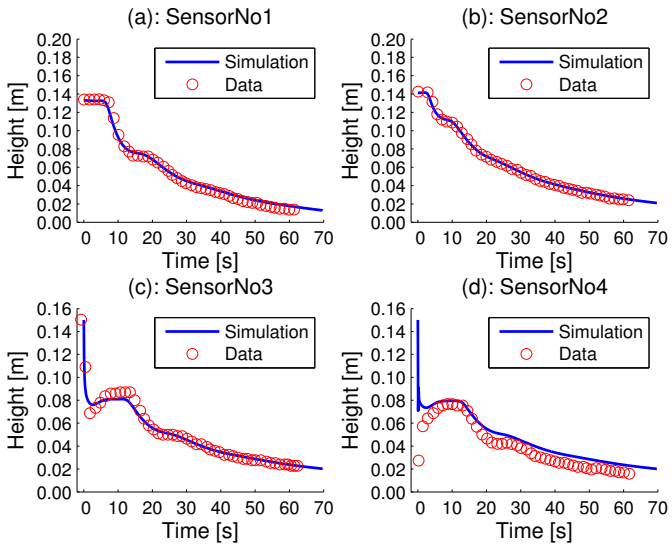

Figure 4.9: Pure simulation for the upstream wave meter locations Amour et al. (2013).

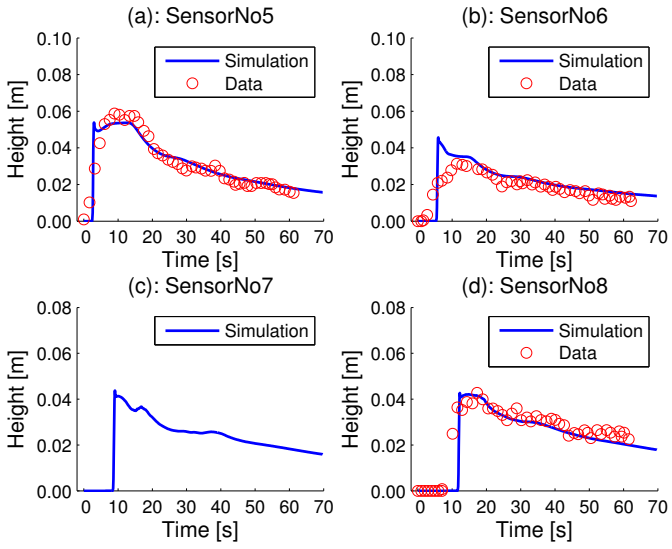

Figure 4.10: Pure simulation for the downstream wave meter locations (Amour et al., 2013).

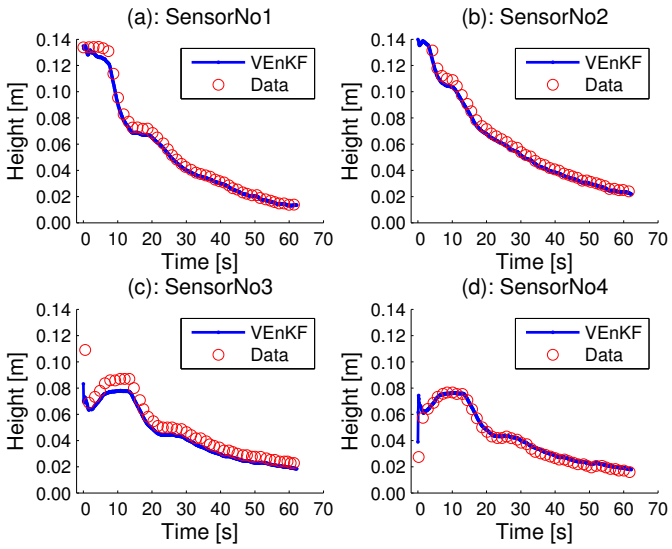

Figure 4.11: VEnKF assimilation for the sensor locations 1 through 4 (Amour et al., 2013).

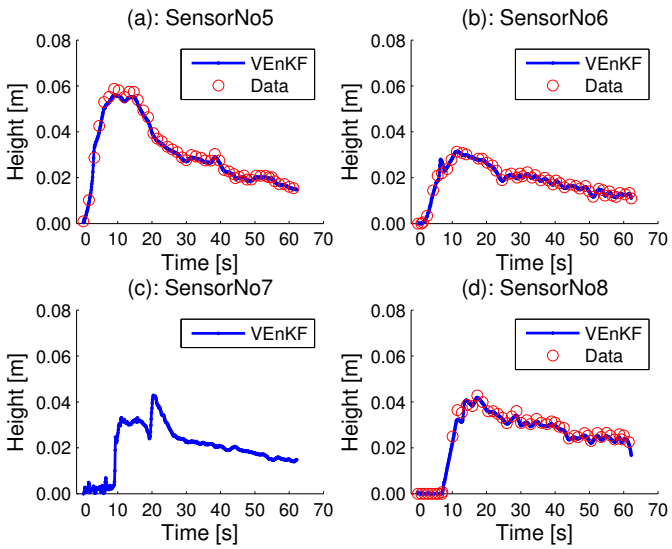

Figure 4.12: VEnKF assimilation for the sensor locations 5 through 8 (Amour et al., 2013).

CHAPTER V

Higher dimensional models in hydrology and limnology

5.1 Motivation

So far, we have introduced VEnKF applications up to 2D small-scale problems. In real application, the emphasis is on 3D large-scale problems. We take a turn into a 3D hydrodynamical-ecological model for regional and shelf-seas (COHERENS). The use of any novel DA should not end up in small-scale (toy) model, and we need to explore the use and performance of the VEnKF in this case too. Very few studies have been conducted in COHERENS with DA. To mention here are; the work of Mano et al. (2015) used traditional DA approach similar to the nudging method where a term is added to the model that nudges a solution towards observations (Kalnay, 2003). The COHERENS model was reinitialized using the initial condition adjusted toward measurement data at every time data are available. Several versions of similar approaches in DA have been studied by Zou et al. (1992); Auroux and Blum (2008); Lei and Hacker (2015). The drawback of the approach in Mano et al. (2015) is that, it does not probabilistically account for model background and its statistics at analysis time, which means that the process does not fully benefit from the DA procedure. The authors in Mano et al. (2015) have still seen improvement in results with this approach. The other study is the work of Ponsar and Luyten (2009); in this work the square root EnKF (SREnKF) has been used. Because of computational demands, the author used a one-dimensional simplified COHERENS model in North Sea location $55^0 30'$ North and $0^0 55'$ East. One-dimensional simplified version of COHERENS has an obvious demerit of not representing the real flow of the ocean, however the author reported improved results with SREnKF which compensate "bad physics"of the model (Ponsar and Luyten, 2009). This gives us an emphasis of the power of the DA procedure in numerical model. In real application one would need to utilize the full features of the model dynamics and its components. We are going to show how VEnKF can work together with COHERENS without any loses of its features.

5.2 3D hydrodynamic model – COHERENS

COHERENS which stands for COupled Hydrodynamical Ecological model for REgioNal Shelf seas, is a 3D multitasking hydrodynamical model intended for coastal and shelf seas, estuaries, lakes, reservoirs which can also be adapted in a similar environment to the mentioned above (Luyten, 2014). The first public source code of COHERENS version 1 (V1) was released in 2000 and has

been actively update since then. The current version of COHERENS (V2.9) is written in FORTRAN 90 with an extensive user documentation with several test applications ready to compile and run. COHERENS contains four main components for simulation:

i. Physical module for solving advection-diffusion equations.

ii. Microbiological module that deals with dynamics of microplankton, detritus, dissolved inorganic nitrogen and oxygen.

iii. An Eulerian sediment module which simulates decomposition and resuspension of inorganic as well as organic substances.

iv. A component with both Eulerian and a Lagrangian transport model for contaminant distributions.

Many more features such as morphology and dredging/relocation have been developed in COHERENS but are not been fully functional for public release (Luyten, 2015).

The COHERENS model equations for the 3D mode feature a continuity equation, momentum equations and temperature and salinity equations. Assumptions used in their derivation can be referred in Luyten (2014). These equations might look similar to the equations for MOD_FreeSurf2D, but the difference is that COHERENS has the vertical components as the third dimension and also has other model equations, for example temperature and salinity. COHERENS supports two types of coordinates system; Cartesian coordinates and spherical coordinates. In this manuscript we will only present COHERENS model equations in Cartesian coordinates:

$$\frac{\partial u}{\partial x}+\frac{\partial v}{\partial y}+\frac{\partial w}{\partial z}=0 \tag{5.1}$$

$$\frac{\partial u}{\partial t}+u\frac{\partial u}{\partial x}+v\frac{\partial u}{\partial y}+w\frac{\partial u}{\partial z}-fv=-\frac{1}{\rho_0}\frac{\partial p}{\partial x}+F_x^t+\frac{\partial}{\partial z}\left(\nu_T\frac{\partial u}{\partial z}\right)+\frac{\partial}{\partial x}\tau_{xx}+\frac{\partial}{\partial y}\tau_{xy} \tag{5.2}$$

$$\frac{\partial v}{\partial t}+u\frac{\partial v}{\partial x}+v\frac{\partial v}{\partial y}+w\frac{\partial v}{\partial z}+fu=-\frac{1}{\rho_0}\frac{\partial p}{\partial y}+F_y^t+\frac{\partial}{\partial z}\left(\nu_T\frac{\partial v}{\partial z}\right)+\frac{\partial}{\partial x}\tau_{yx}+\frac{\partial}{\partial y}\tau_{yy} \tag{5.3}$$

$$\frac{\partial p}{\partial z}=-\rho g \tag{5.4}$$

$$\frac{\partial T}{\partial t}+u\frac{\partial T}{\partial x}+v\frac{\partial T}{\partial y}+w\frac{\partial T}{\partial z}=-\frac{1}{\rho_0 c_p}\frac{\partial I}{\partial z}+\frac{\partial}{\partial z}\left(\lambda_T\frac{\partial T}{\partial z}\right)+\frac{\partial}{\partial x}\left(\lambda_H\frac{\partial T}{\partial x}\right)+\frac{\partial}{\partial y}\left(\lambda_H\frac{\partial T}{\partial y}\right) \tag{5.5}$$

$$\frac{\partial S}{\partial t}+u\frac{\partial S}{\partial x}+v\frac{\partial S}{\partial y}+w\frac{\partial S}{\partial z}=\frac{\partial}{\partial z}\left(\lambda_T\frac{\partial S}{\partial z}\right)+\frac{\partial}{\partial x}\left(\lambda_H\frac{\partial S}{\partial x}\right)+\frac{\partial}{\partial y}\left(\lambda_H\frac{\partial S}{\partial y}\right) \tag{5.6}$$

where (u, v) are the horizontal components of the flow velocity, w is the vertical component of the flow velocity, $f = 2\Omega\sin(\phi)$ is the Coriolis frequency, where $\Omega = \pi/43082$ radians/sec is the frequency of rotation of the earth, p is pressure, ρ is density, ρ_0 is a uniform reference density, g is the acceleration due to gravity, (F_x^t, F_y^t) are the components of the astronomical tidal force, ν_T and λ_T are the vertical turbulent diffusion coefficients, ν_H and λ_H are the horizontal turbulent diffusion coefficients, τ_{ij} is the horizontal friction tensor, T is potential temperature (not in-situ temperature), which is defined as temperature of a fluid parcel, moved adiabatically to a certain level (Luyten,

2014), I is the solar irradiance within the water column, c_p is the specific heat capacity of sea water at constant pressure and S is the salinity (Luyten, 2014). In the current version of COHERENS (V2.9), the formation of ice is not allowed, therefore the temperature must be higher than the freezing point. More details on the model equations and their parameterization can be found in Luyten (2014).

$$T > \alpha_f S\ , \quad \alpha_f = -0.0575\ ^0\text{C/PSU} \tag{5.7}$$

5.3 Numerical methods in COHERENS

The solver in COHERENS uses conservative finite differences to discretize the model equations in space. With this, the Arakawa C-grid (see Figure 4.2 for 2D Arakawa C-grid) is employed for horizontal discretization (Luyten, 2014). In the first implementation of COHERENS, the momentum equations were solved with a mode-splitting method as described in Blumberg et al. (2013). The method has two phases; the first one solves the depth-integrated momentum equations and continuity equations for the barotropic mode with a small time step not to violate CFL stability condition for surface gravity waves. The second one is to solve the 3D momentum and scalar transport equations for the baroclinic mode with a larger time step. A predictor and corrector step are used to match the results obtained from depth-integrated equations and the 3D mode equations. In the current implementation, COHERENS solves the momentum equations with the semi-implicit scheme of Casulli and Cheng (1992). The benefit of this method is that solving the depth-integrated momentum equations is not needed. The CFL stability condition is relaxed by dealing with the term that disturbs the barotropic mode in an implicit way (Luyten, 2014). An explicit predictor step is first calculated, then followed by an implicit corrector step for velocity corrections. More details on the numerical method steps and procedures can be referred in Luyten (2014). COHERENS is a very flexible package which allow users to choose varieties of schemes and parameters for different settings. There are more than 80 switches in COHERENS (Luyten, 2014). One can choose for example to activate a turbulence scheme, choose model grid type, include model forcing data, use MPI, enable a biological module, set user output types, activate drying and wetting algorithm and many more by simply activating appropriate switches.

CHAPTER VI

Non-intrusive VEnKF implementation to COHERENS

6.1 Data assimilation in hydrology and limnology

One application for DA in hydrology is an error forecasting procedure, see for example in Madsen and Skotner (2005); Reichle et al. (2008); Moradkhani et al. (2005). The most common way to apply DA in hydrological models is to update the initial conditions based on the prior information of the model and the measurements; as an example, see the work of Amour et al. (2013); Heemink and Metzelaar (1995). DA in hydrology and other fields have proven to give better forecasts when compared to pure simulations, as can be seen in Ponsar and Luyten (2009); Auvinen et al. (2010); Solonen et al. (2012); Amour et al. (2013) for example. The task of determining best parameters for the model and observations remains a big challenge and may cause even deterioration of results (Reichle et al., 2008). A precise representation of the internal oscillations of a 3D hydrological model is critical to successful simulations (Luyten et al., 2003). But, with extra information from measurements this tendency can be captured and corrected (Amour et al., 2013; Ponsar and Luyten, 2009).

Use of DA in hydrology has become apparent in parallel with the traditional approach of parameter estimation of the model. Several DA methods have been utilized in the fields of hydrology and limnology. The performance of assimilation methods depends on the method employed. Despite COHERENS being used by many researchers and institutions in the field of hydrology and limnology, DA has not been often carried out with it. One of the few such works was studied with the simplified 1D COHERENS model of a North Sea by Ponsar and Luyten (2009), whose results with SREnKF were promising, but depend much on ensemble initialization (Ponsar and Luyten, 2009).

EKF has a long history in hydrology research works (Clark et al., 2008). But, its practical implementation has been a major obstacle with high dimensional models. EKF has to invert and operate a big matrix of the order 10^7 by 10^7, which is an obstacle on current computing platforms. Non-linearity in the model has also been another challenge for EKF, as one has to produce the tangent linear and adjoint codes which are not always available for the model and are tedious to construct and maintain.

The EnKF has been widely used in hydrology, because of its non-linear error covariance propagation in time, for example in Xie and Zhang (2010); Kim et al. (2014a); Komma et al. (2008). In Clark et al. (2008), streamflow observations have been used to update model state in a distributed hydrological model using EnKF.

Water quality is an important phenomenon to be studied with both modeling and measurements but it has not been covered much in DA literature (Kim et al., 2014a,b). In Kim et al. (2014a), a study of algal bloom dynamics in a river with the EnKF was performed. The model had to be run with a small ensemble size due to heavy computation in 3D hydrodynamics models. Small ensemble sizes make the quality of covariance error propagation uncertain (Kim et al., 2014a; Komma et al., 2008). Soil moisture has been also an active field of study with the use of EnKF, see for example Komma et al. (2008); Clark et al. (2008). In the work of Clark et al. (2008), the EnKF underestimated the forecast error covariance for small ensemble sizes, but gave reasonable results with bigger ensemble sizes, which suggests significance of dynamic error covariance propagation (Clark et al., 2008).

VEnKF is still a novel candidate in DA but it has proven to be competitive in many aspects. As stated in Solonen et al. (2012), the VEnKF needs neither tangent linear nor adjoint codes. We are convinced that, it is a good candidate in hydrological models. In the work of Amour et al. (2013), VEnKF has demonstrated its ability to forecast water heights in a dam-break experiment of Martin and Gorelick (2005), which was first experimented by Bellos et al. (1991). Results were convincing enough to carry out more complex assimilation tasks with VEnKF, taking into account another advantage, that VEnKF can be easily parallelized.

6.2 Motivation

Two factors may be considered in DA implementation. First, in many cases DA calculations are more expensive than the model evolution calculations. To address this issue, several DA schemes have been introduced with computationally better algorithms, some of these were mentioned in Chapter 2. Second, if the computations are fairly affordable then one has to incur a cost of coupling the DA scheme with the model. In an advanced multi-task model, the coupling with DA is a tedious task. A limited number of studies have been made to address this difficulty with an affordable and robust solution. In some articles, the implementation of an offline DA procedure has been developed with the emphasis of rapid implementation rather than efficiency of the computations (see Browne and Wilson (2015) for example). In Nerger (2004); Browne and Wilson (2015), a message passing interface (MPI) functionality has been introduced to couple DA method with the model. Clear advantage of all these implementations is that the model code is minimally changed, one has only to find the right place in the model code to insert few lines of code for the coupling. One disadvantage is that, by introducing MPI into the model we increase the overhead to call the DA as a separate routine callable by the model. Similar procedure has been introduced in Nerger and Hiller (2013); Nerger and Kirchgessner (2015) with two possible alternatives, an offline mode where, the communications between the model and the DA is done through files. Another alternative is to use the online mode, where the communications between the model and the DA is done by special routine calls, where all codes are compiled into a single program, while the model code remains intact.

As it has been mentioned, the cost of making a wrapper code for the DA scheme to the model can be very expensive, and when the model code documentation is not available the situation turns to worse. COHERENS as 3D multipurpose software for shallow water and deep sea has not been much studied with DA. In Ponsar and Luyten (2009), an EnSKF has been coupled with a 1D simplified COHERENS to assimilate North sea dynamics, where the results were significantly improved. The simplification of a 3D model to 1D has an obvious disadvantage of missing vertical and horizontal dynamics. We here present a way similar to the one introduced in Nerger and Kirchgessner (2015);

Nerger and Hiller (2013) with full-blown COHERENS model dynamics. We believe that, exploiting the possibility of coupling COHERENS with DA without a major code change, could provide an cheaper way for coupling DA schemes in COHERENS as well as other models of interest.

6.3 Non-intrusive algorithm

Implementation of an ensemble type DA scheme to a coupled model system is tedious and needs a lot of technical work. To alleviate this, we present a non-intrusive way of implementation of the DA (VEnKF in this manuscript) scheme to a coupled model system (COHERENS). In this way the model code remains untouched and the communication between the model (COHERENS) and the assimilation scheme (VEnKF) method is made possible through input and output devices (files). In particular for COHERENS, one has to write and read the files in COHERENS standard format where COHERENS would read the files without any complains. The non-intrusive VEnKF algorithm is presented in Figure 6.1.

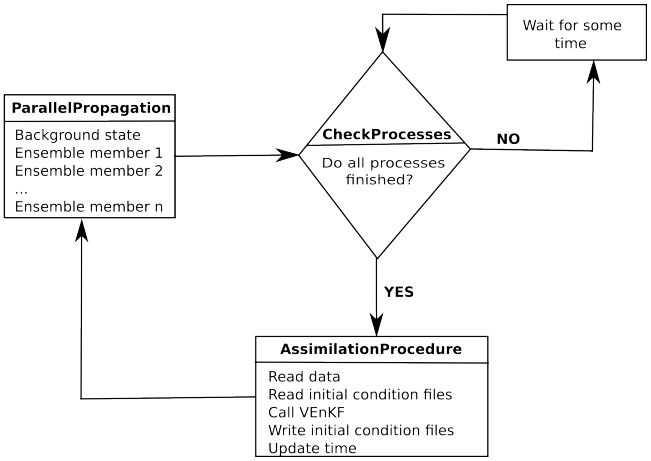

Figure 6.1: Non-intrusive VEnKF algorithm.

6.4 Case study: Lake Säkylän Pyhäjärvi

In this manuscript we will explore a non-intrusive VEnKF application to hydrodynamic flow in lake Säkylän Pyhäjärvi, which is located in the South-Western part of Finland. The lake has a total water area of 154 km^2 with mean water depth of 5.4 m (Huttula, 1994), where the deepest point is 25 m deep (Räsänen et al., 1992). Figure 6.2 is a map of the lake Säkylän Pyhäjärvi, the lake has three openings, one in the southern part; river Yläneenjoki, one in the eastern part; river Pyhäjoki and the last one in the northern part; river Eurajoki. The direction of the flow is shown by the arrows in the map. With our limited computational resources, we are forced to use 1 km grid resolution. The simulation was run with 20 vertical layers. The time step of the model was set to 20 s, and model fields were written after every 6 hours from the beginning of the simulation. It is worth to

mention that in this work we did not make a new COHERENS setup, instead we have adopted the setup made in Mano et al. (2015).

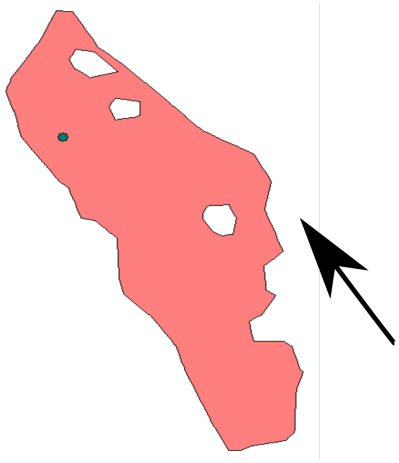

Figure 6.2: Map of lake Säkylän Pyhäjärvi located in South West of Finland. The green dot shows the location of the automatic station. The flow direction is shown by the arrow.

6.5 Assimilation of artificial temperature data

Before we apply VEnKF to real data, we first take a common practice in data assimilation, assimilating with artificial temperature data. The advantage is that, it is easy to debug when something goes wrong, which is not easy for the real data. Also the statistics of the results can be well computed based on the true solution. With this experiment, we have made artificial temperature measurements by solving the COHERENS model for 5 days, from May 15 2009 at noon to May 20 2009 at noon. The initial temperature was set to be 10.1 deg C as recorded in the Finnish Environmental Institute (SYKE) Hertta database as the vertical average at the deepest point between 10 and 20 May 2009 (Mano et al., 2015). To create artificial temperature measurements we generated normally distributed noise with mean 0 and variance $\sigma_o^2 = 0.15 \times 3.6414723$ then add this to the COHERENS temperature fields. For the matter of testing, we have assumed data to be observed for all lake layers and all grids. The observation error covariance was assigned a value $10\sigma_o^2\mathbf{I}$, the model covariance error was assumed equal to the observation covariance error.

The assimilation has been carried out after every 6 hours. Fine tuning of line search parameters in the Wolfe conditions was assured for better convergence in the LBFGS optimizations. Maximum number of iterations in LBFGS was set to 100, with maximum number of stored vectors as 20. The VEnKF assimilation has been run with 10, 20, 50 and 100 ensemble members.

6.5.1 Results and analysis

The aim of the artificial experiment is to test the performance of the algorithm and code execution. If everything goes successfully, then we are ready for the real assimilation task, where measurements and the prior are not correlated in any way. The results of the artificial experiment show that the non-intrusive VEnKF algorithm works well and gives expected results. The convergence of the LBFGS minimization was monitored and found to be consistent for the entire period of assimilation. The LBFGS converges between 10 and 60 iterations. For this test case, we compare the COHERENS model solution called the truth in this case and the VEnKF estimates by plotting the root mean square error (RMSE) plots and relative error (defined by Equation (6.1)) plots.

$$[\text{RelativeError}]_k = \frac{||\hat{\xi}_k - \xi_k^{\text{truth}}||}{||\xi_k^{\text{truth}}||} \tag{6.1}$$

where ξ_k^{truth} and $\hat{\xi}_k$ represents the truth and assimilation estimates at time point k, respectively.

The results in Figure 6.3 shows that the VEnKF has captured fairly well the temperature dynamics in the period of assimilation. In Figure 6.4, the relative error plot is given and it shows a good convergence of error after some time of VEnKF learning from the observation sets. In Figure 6.5, we see that the RMSE is bounded, which is a good sign for assimilation scheme behavior. With reference to these results we have a courage to move to the real data case.

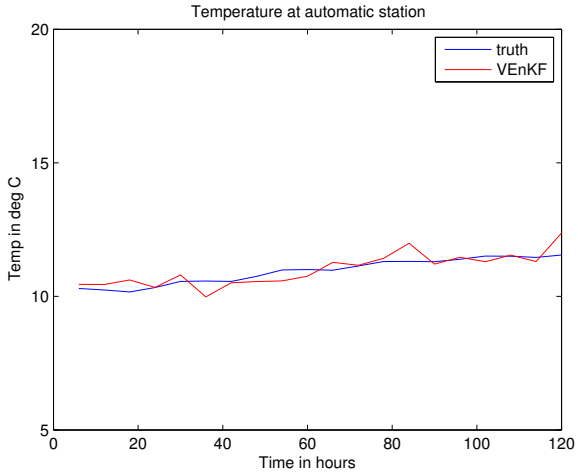

Figure 6.3: The true temperature values compared to the VEnKF estimates for 120 hours of simulation from May 15 to May 20, using 100 ensemble members.

6.6 Assimilation of total suspended matter

In this experiment, we assimilate with VEnKF the total suspended matter (TSM) in lake Säkylän Pyhäjärvi. The TSM is derived from the turbidity and chlorophyll-a 6 days MERIS satellite images

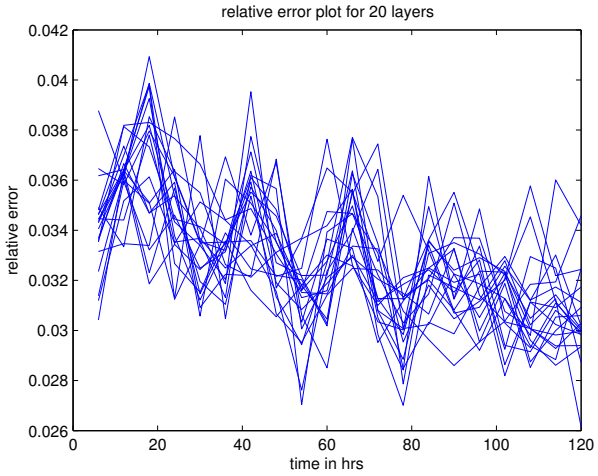

Figure 6.4: The relative error plot for all layers, using 100 ensemble members.

for the lake Säkylän Pyhäjärvi. The images were provided by SYKE and taken at noon on May 16, June 1, June 8, June 18, June 21, June 26, July 6 2009. The turbidity data contains the effect of organic substances, which has been removed by using Equation 6.2 (Mano et al., 2015).

$$\text{TSM}_{(\text{no biomass})}(i,j) = \frac{1}{1.09}\big(\text{Tur}(i,j) - 0.0449\big) - \frac{1}{10}\text{Chl}(i,j) \tag{6.2}$$

where TSM stands for total suspended matter concentration without biomass, Tur is turbidity concentration from the satellite image and Chl is the Chlorophyll-a concentration data from the satellite image (Mano et al., 2015). Because of the spatial resolution of 300 m, MERIS images usually do not provide beneficial information for small lakes and straits (Malve et al., 2016). These MERIS images were interpreted using the Boreal lake processor (Doerffer and Schiller, 2008), as in Malve et al. (2016). The satellite data are normally describe the top surface layer, which causes the assimilation process to have more or less no information from the bottom layers. The model has been initialized with TSM values of 0 mg/l, at May 15 noon and run for 24 hrs (spin-up phase), then the model was initialized with the TSM values of 2.5 mg/l at May 16 noon (same setting as in Mano et al. (2015)), which is then run for as long as observations are available. The VEnKF has been run with 10, 30 and 50 ensemble members using the same VEnKF parameters of the artificial experiment.

6.6.1 Results and analysis

The idea of this experiment is to implement a non-intrusive VEnKF algorithm on a large-scale high dimensional model. In this case COHERENS, and examined its performance. The algorithm proved to be stable and robust, as there was no change in model code except for few lines to introduce few flags and parameters written to file and read by both COHERENS and VEnKF. The convergence of the method was observed and controlled; converging between 10 and 80 out of 100 LBFGS iterations with the gradient norm between 10^{-3} and 10^{-5}.

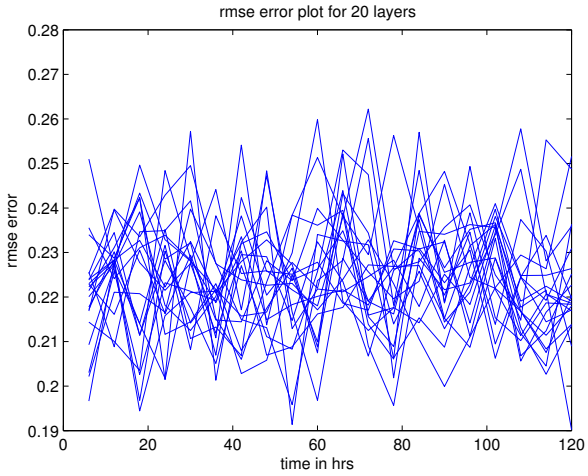

Figure 6.5: The root mean square error plot for all layers, using 100 ensemble members.

COHERENS can optionally run with full 3D mode (3D mode) or with partial 3D mode. Here we present results for 3D mode and a partial 3D mode where we run 15 2D COHERENS time steps between every 3D time step (2D mode). In Figures 6.6 – 6.11, we have plotted the assimilation outcomes with ensemble sizes of 10, 30 and 50, respectively, with both 3D mode (Figures 6.6 – 6.8) and 2D mode (Figures 6.9 – 6.11) visualizing the prior state of the TSM, derived satellite data for TSM and the VEnKF estimates for TSM.

The results from Figures 6.6, 6.7 and 6.8 show that ensemble sizes 10, 30 and 50 used in this experiment are hard to distinguish. However from these figures we see that VEnKF output is a result of combining the prior and the measurements as it also follows directly from the definition of a Kalman Filter.

VEnKF results are compared with the measurements collected at the automatic station shown with a green dot in the map (Figure 6.2). The instrument was put at a depth of 1 m below the surface, the measurements were available from May 18 to July 7 2009 for every 1 hour. To make reasonable comparison between VEnKF and the automatic station measurements we make plots for the surface layer only. The VEnKF captured reasonably well the time series of TSM. In Figures 6.12 – 6.13, the VEnKF captured the time series of turbidity in many parts of the assimilation period except at the beginning of the assimilation, as the first satellite data comes in June 1 2009. The results suggest that the mode of the run is not very significant since the satellite images contain information on the surface of the lake only. The results of TSM VEnKF estimate with 50 ensemble members look a little better than those with 30 ensemble members (refer Figures 6.12 – 6.13) in the sense of quality of estimates. Consequently, it suggests that even low ensemble sizes are enough to capture the error propagation of the model state.

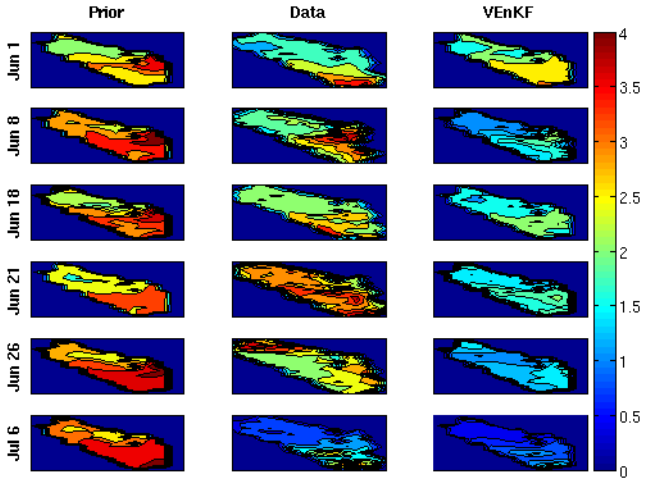

Figure 6.6: The prior state, satellite data and the VEnKF estimates for the assimilation on June 1, 8, 18, 21, 26 and July 6 using 10 ensemble members in 3D mode.

6.7 Remarks

We did not expect much from the 1 km grid resolution used in the assimilation. We have got assurance that the algorithm is working, and can be used to search better results by improving for example grid resolution, which in the other hand is hindered by computational resources. The results for both 2D and 3D mode were close in terms of the estimates, this is explainable by the fact that, satellite images provide data for surface layer only, therefore pass no information about the bottom layers to the VEnKF. The simulation had 20 vertical layers, so the measurements represented by only $1/20$ in the state vector. Thus, the assimilation represented sparse case.

The VEnKF has been run with different ensemble sizes, we have found that, the use of higher ensemble size is not significant in this application. Extra ensemble members add little contribution in the performance. This finding is crucial as now researchers are working in the development of non-intrusive reduced order hybrid and ensemble DA methods, see for example the work of Heemink et al. (2001); Xiao et al. (2016). In Heemink et al. (2001); Cosme et al. (2010) for example, the computationally efficient EnKF and square root Ensemble Smoother were proposed, both use reduced-rank approximation for the error covariance matrix which is estimated using singular value decomposition. The main idea behind the reduced order modelling is to save tremendous computational time needed by full-blown model, if this can be achieved together with low ensembles hybrid method, it would be good achievement in the field of modelling and assimilation. Another work presented by Madaus and Hakim (2015) which is closely related to the reduced order modelling, whereby the forecast fields are adjusted without running the full dynamical model. EnKF is used to correct forecast variables based on observation and ensemble covariances and tested with ECMWF and CMC ensemble forecasts.

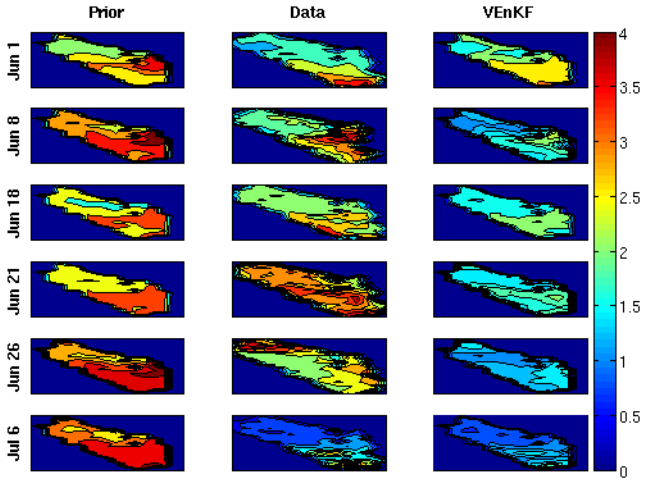

Figure 6.7: The prior state, satellite data and the VEnKF estimates for the assimilation on June 1, 8, 18, 21, 26 and July 6 using 30 ensemble members in 3D mode.

The derived TSM concentration from the satellite images contains errors, both by removing the effect of organic matters in Equation (6.2) and the image processing itself. It would be interesting to add more measurements information by using automatic station data as well in the assimilation. The use of higher resolution grid is an important step towards improving assimilation performance. With the current computer resources, this was not possible because all simulations have been run with normal resources personal computers. The use of supercomputer can not be avoided in any real and challenging simulations.

Wrapper code implementation for the DA with the multipurpose model has been always cumbersome. The successful implementation of the non-intrusive VEnKF algorithm gives us hope for more work to be carried out to improve the performance of the non-intrusive algorithm. We do not claim that the non-intrusive method presented in this manuscript as the best, it has some drawback in efficiency, one; the model and the DA method are called by the outside shell program, in which case at every beginning of the analysis time both the model and VEnKF have to be initialized. The initialization of the two can take a significant amount of computation time when the assimilation period is shorter and over a long duration. Two; controlling the run with the outside program may miss some functionalities which are available in the model/DA programming code. Nonetheless, the use of external program has an advantage that the model code and DA code can be from different programming languages, because they do not interact to each other through codes but through disk files.

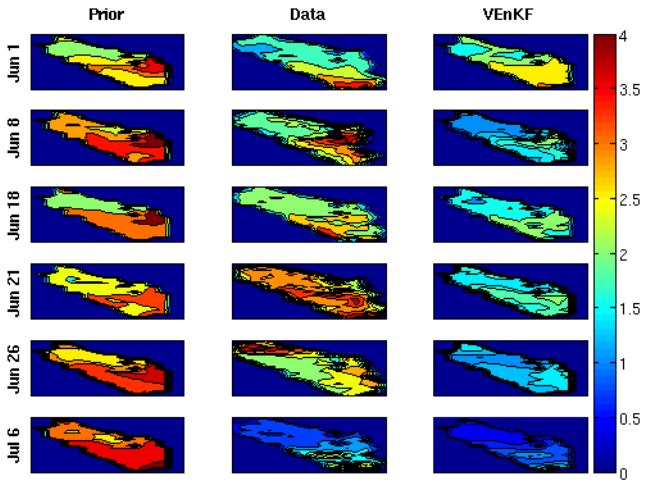

Figure 6.8: The prior state, satellite data and the VEnKF estimates for the assimilation on June 1, 8, 18, 21, 26 and July 6 using 50 ensemble members in 3D mode.

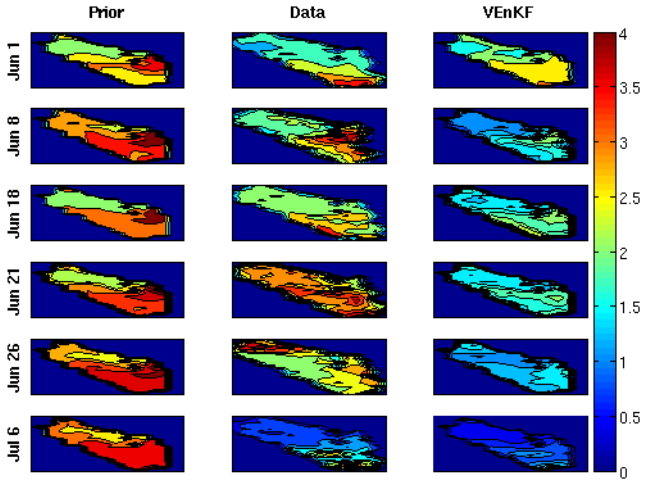

Figure 6.9: The prior state, satellite data and the VEnKF estimates for the assimilation on June 1, 8 18, 21, 26 and July 6 using 10 ensemble members in 2D mode.

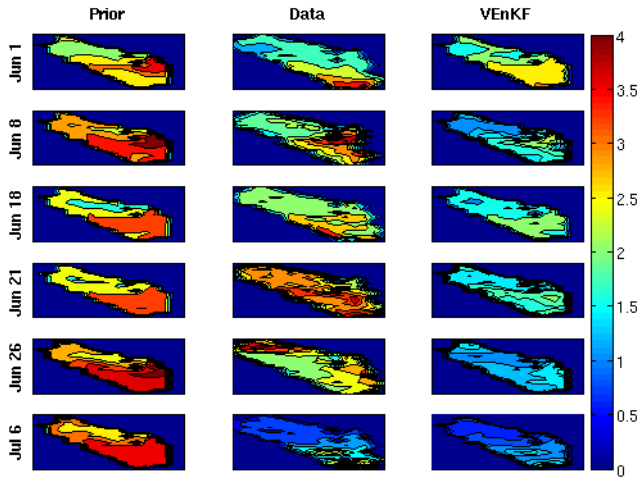

Figure 6.10: The prior state, satellite data and the VEnKF estimates for the assimilation on June 1, 8, 18, 21, 26 and July 6 using 30 ensemble members in 2D mode.

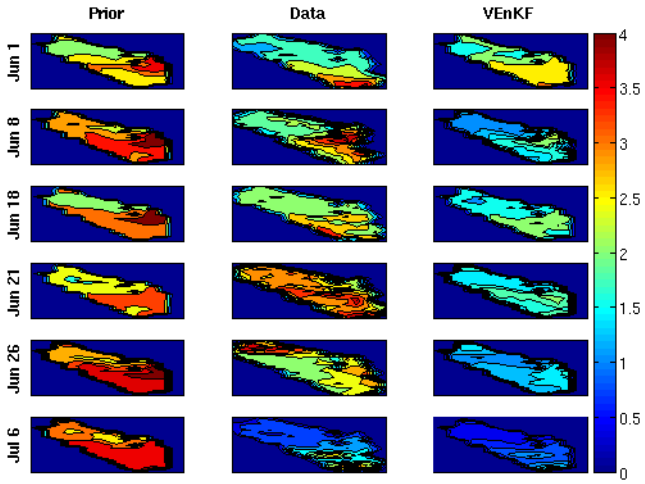

Figure 6.11: The prior state, satellite data and the VEnKF estimates for the assimilation on June 1, 8, 18, 21, 26 and July 6 using 50 ensemble members in 2D mode.

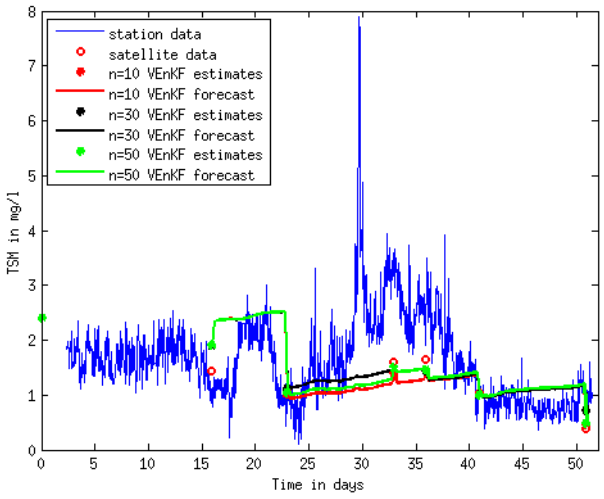

Figure 6.12: VEnKF assimilation of the TSM for surface layer from May 16 to July 6 2009 at the automatic station using 10, 30 and 50 ensemble members in 2D mode. VEnKF estimates are the TSM values at the assimilation time while VEnKF forecasts is the TSM trajectory of the model using VEnKF estimates as the initial conditions.

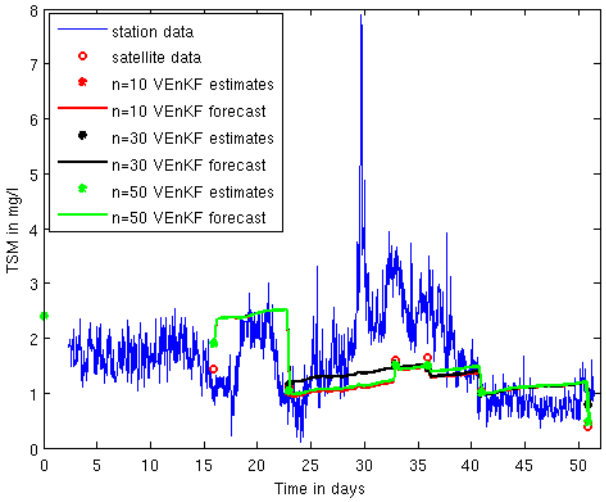

Figure 6.13: VEnKF assimilation of the TSM for surface layer from May 16 to July 6 2009 at the automatic station using 10, 30 and 50 ensemble members in 3D mode. VEnKF estimates are the TSM values at the assimilation time while VEnKF forecasts is the TSM trajectory of the model using VEnKF estimates as the initial conditions.

CHAPTER VII

Conclusions and Discussion

In this manuscript, a novel data assimilation method namely Variational Ensemble Kalman Filter (VEnKF) has been studied with a range of medium and large-scale problems. Firstly, the VEnKF uses the advantage of ensemble methods to propagate an error covariance matrix over time using a nonlinear model. Therefore it avoids many drawbacks which are sometimes troubling ensemble methods. One to mention is the filter inbreeding problem which happens when an error covariance matrix estimate is no longer representing the true variability of the estimate. This usually results in filter divergence. In VEnKF this is securely controlled by making new samples every time measurement data is available. Secondly, the VEnKF uses the advantage of control theory to find the estimate of the filter using a cost function which minimizes the total covariance weighted distance from the estimate to the prior and from the estimate to the measurement. In this case, we have avoided the heavy computational complexity associated with by ensemble methods and Kalman filter methods in general. The classical Kalman filters have to conduct matrix inversion of large full matrices and, a memory is needed to store a matrix of order of $10^7 \times 10^7$. The VEnKF introduction has been inspired by the Variational Kalman Filter (VKF) which also has computational challenges as it needs tangent linear and adjoint codes in its implementation. These are usually hard to make and maintain, however when available they can be used for several DA schemes. VEnKF in this aspect has positive gain over VKF, as it does not use any of these challenging codes. The results for the test applications used to test VEnKF were positive. The EKF has been used as a de facto method to be compared with the novel methods. In the test applications, the results for EKF were matched well with the results of the VEnKF with a large number of ensemble members. For the case of the 40 dimensional Lorenz 95, 40 ensemble members gave almost comparable results. This is seconded by the fact that ensemble methods needs dozen of ensemble members to behave well, no matter how small is the model state vector. For the heat equation application, the RMSE plot results of VEnKF were better than that of the 3D-Var with constant background covariance.

Apart from the test applications, the first real case application for the VEnKF has been introduced in Amour et al. (2013). The VEnKF has been successfully applied to a two-dimensional shallow water model simulating a dam-break experiment. The results of the assimilation were convincing, as they represent the natural flow of water compared to the pure simulation presented in Martin and Gorelick (2005). In pure simulation some numerical artifacts could be clearly seen. For example, smoothness of the flow and wave jumps at the beginning of the simulation. All these artifacts have been corrected by the VEnKF with the help of measurements. The challenge of this assim-

ilation was mainly the sparsity of the measurement data. The sparsity of data in space was more problematic to the VEnKF. To make stable assimilation we have interpolated water height data in both time (using spline piecewise polynomials) and in space (using a Gaussian Kernel). It was then possible to conduct data assimilation at every computational time step, even this procedure might be computationally a big burden for large-scale problems assimilation. VEnKF has shown positive achievements for 2D large-scale problems.

The problem of coding the DA scheme and model are not the only things to worry about. Coupling the two might be more difficult than coding each of them separately especially when the two are not prepared for the coupling at the design stage. The wrapper code for the DA scheme and the model has been a big challenge in assimilation use. In some cases model documentation is not available or available but with minimal information. To avoid these difficulties we have adapted a non-intrusive implementation of the VEnKF to the COHERENS model. In this implementation the model code does not communicate with the DA through computer codes, but through input and output devices. Therefore the model code change is very minimal, only few lines to tell the two codes to read and write initial condition files and to identify the first DA scheme call for ensemble initialization. At every analysis time the model writes its final condition which is then read and updated by the DA scheme so as to be used as the initial condition next. We only need to implement correctly the reading and writing of these files. We have achieved this implementation using an external program which controls both the COHERENS and the VEnKF runs. We do not claim that this is the best way to couple the two, but we believe it is a robust and painless approach.

One attractive feature of ensemble methods is their flexibility to run in parallel. This has been simply activated with the non-intrusive approach by just asking the control program to wait for all the processes to finish before the VEnKF is called. In some cases, there are ready-made codes for both model and the DA scheme, but may be they are written in different programming languages. To couple the two using wrapper codes might be very expensive, but with the non-intrusive approach presented in this manuscript is straightforward, and it does not matter which programming language is used in either of them. What has to be done when we need to implement the best possible DA scheme to a model is to test several available DA schemes. This can be a tedious job if we are going to write wrapper codes for each of the DA schemes to the model. For this reason the non-intrusive approach can be used as a benchmark testing platform for several DA schemes to the model. The other side of the coin for this approach is its additional overhead in model and DA scheme initialization. At each assimilation cycle, the model and the DA scheme need to be initialized. These initializations can consume a significant amount of computational time and resources especially when the assimilation is frequently performed and for longer periods of time.

For 3D large-scale problems, VEnKF has been implemented with the multi-purpose hydrodynamic model COHERENS using the non-intrusive approach. The assimilation scheme was stable in the entire period of assimilation. However the results were not good enough to claim best performance. The poor performance can be explained by the fact the measurement data was sparse for the VEnKF to learn the pattern of the total suspended matter (TSM) dynamics in our test case. These data were derived from MERIS satellite images, which usually depict the information on the surface of the lake. Therefore, VEnKF did not have any information on bottom layer flows. Data sparsity is one of the challenging reasons that makes DA schemes to fail. These satellite data were sparse in time and space. With respect to time sparsity, the data were only available for 7 days in the period of 52 days. The most provocative sparsity is the space sparsity, in this case only 1/20 of the model state vector were available. The good point for this implementation is that the VEnKF worked smoothly and the minimization algorithms were converging nicely. With the developing technology in data

collection, automatic stations might be useful to provide almost real time measurements. These data are seldom used in routine DA (Daescu and Navon, 2003) are usually automatically collected and are available in good frequency, however these stations might need extra resources to maintain.

It has been shown that, running a full-blown model in some cases is computationally demanding with the available resources. There is growing attention to reduced order modelling, whereby a model is run with a simplified version with reasonable assumptions. Referring the VEnKF results with COHERENS, it has been shown that the use of very large ensemble sizes do not necessarily provide better results. There is a limit on ensemble sizes after which the additional members contribute very little to the analysis. For example the case of 30 and 50 ensemble members in the assimilation of TSM in the lake Säkylän Pyhäjärvi were fairly identical. In the presented non-intrusive approach, reducing the number of ensemble members reduces linearly the computational time required to run the data assimilation, because every ensemble member is run independently and as a full-blown model run on the specified time interval. This outcome might be useful in the development of non-intrusive reduced order modeling. The resulting DA algorithm can be run with a simplified model version (for example reduced order model) using possible low ensemble members with the non-intrusive DA ensemble method approach.

Acton, Q. A., 2012. Advances in Information Technology Research and Application: 2011 Edition. ScholarlyEditions.
URL https://books.google.fi/books?id=WdcRZQ5BDqsC

Aliparast, M., 2009. Two-dimensional finite volume method for dam-break flow simulation. International Journal of Sediment Research 24 (1), 99–107.

Amour, I., 2008. On Variational Ensemble Kalman Filtering. Master Thesis, Lappeenranta University of Technology, Finland.
URL https://www.doria.fi/bitstream/handle/10024/42026/nbnfi-fe200806161566.pdf?sequence=1

Amour, I., Mussa, Z., Bibov, A., Kauranne, T., 2013. Using ensemble data assimilation to forecast hydrological flumes. Nonlinear Processes in Geophysics 20 (6), 955–964.

Anderson, J. L., 2007. An adaptive covariance inflation error correction algorithm for ensemble filters. Tellus A 59 (2), 210–224.

Andersson, E., Haseler, J., Undén, P., Courtier, P., Kelly, G., Vasiljevic, D., Brankovic, C., Gaffard, C., Hollingsworth, A., Jakob, C., Janssen, P., Klinker, E., Lanzinger, A., Miller, M., Rabier, F., Simmons, A., Strauss, B., Viterbo, P., Cardinali, C., Thépaut, J., 1998. The ECMWF implementation of three-dimensional variational assimilation (3D-Var). III: Experimental results. Quarterly Journal of the Royal Meteorological Society 124 (550), 1831–1860.

Arakawa, A., Lamb, V. R., 1977. Computational Design of the Basic Dynamical Processes of the UCLA General Circulation Model. In: Chang, J. (Ed.), General Circulation Models of the Atmosphere. Vol. 17 of Methods in Computational Physics: Advances in Research and Applications. Elsevier, pp. 173–265.

Arias, M. L., Corach, G., Maestripieri, A., 2015. Range additivity, shorted operator and the Sherman-Morrison-Woodbury formula. Linear Algebra and its Applications 467, 86–99.

Auroux, D., Blum, J., 2008. A nudging-based data assimilation method: the Back and Forth Nudging (BFN) algorithm. Nonlinear Processes in Geophysics 15 (2), 305–319.

Auvinen, H., Bardsley, J. M., Haario, H., Kauranne, T., 2009. Large-scale Kalman filtering using the limited memory BFGS method. ETNA. Electronic Transactions on Numerical Analysis [electronic only] 35, 217–233.

Auvinen, H., Bardsley, J. M., Haario, H., Kauranne, T., 2010. The variational Kalman filter and an efficient implementation using limited memory BFGS. International Journal for Numerical Methods in Fluids 64 (3), 314–335.

Baghlani, A., 2011. Simulation of dam-break problem by a robust flux-vector splitting approach in Cartesian grid. Scientia Iranica 18 (5), 1061–1068.

Bárcena, J. F., García, A., García, J., Álvarez, C., Revilla, J. A., 2012. Surface analysis of free surface and velocity to changes in river flow and tidal amplitude on a shallow mesotidal estuary: An application in Suances Estuary (Nothern Spain). Journal of Hydrology 420–421, 301–318.

Bardsley, J. M., Solonen, A., Parker, A., Haario, H., Howard, M., 2013. An ensemble Kalman filter using the conjugate gradient sampler. International Journal of Uncertainty Quantification 3 (4), 357–370.

Barker, D. M., Huang, W., Guo, Y. R., Bourgeois, A. J., Xiao, Q. N., 2004. A Three-Dimensional Variational Data Assimilation System for MM5: Implementation and Initial Results. Monthly Weather Review 132 (4), 897–914.

Bates, P. D., Anderson, M. G., 1993. A Two-Dimensional Finite-Element Model for River Flow Inundation. Proceedings of the Royal Society of London A: Mathematical, Physical and Engineering Sciences 440 (1909), 481–491.

Bellos, C. V., Soulis, J. V., Sakkas, J. G., 1991. Computation of two-dimensional dam-break-induced flows. Advances in Water Resources 14 (1), 31–41.

Bergthórssonz, P., Döös, B. R., 1955. Numerical Weather Map Analysis. Tellus 7 (3), 329–340.

Bertino, L., Evensen, G., Wackernagel, H., 2003. Sequential Data Assimilation Techniques in Oceanography. International Statistical Review 71 (2), 223–241.

Bishop, C. H., Etherton, B. J., Majumdar, S. J., 2001. Adaptive Sampling with the Ensemble Transform Kalman Filter. Part I: Theoretical Aspects. Monthly Weather Review 129 (3), 420–436.

Blumberg, A. F., Mellor, G. L., George, L., 2013. A Description of a Three-Dimensional Coastal Ocean Circulation Model. American Geophysical Union, Ch. Three-Dimensional Coastal Ocean Models, pp. 1–16.

Bocquet, M., Sakov, P., 2012. Combining inflation-free and iterative ensemble Kalman filters for strongly nonlinear systems. Nonlinear Processes in Geophysics 19 (3), 383–399.

Bonnans, J. F., Gilbert, J. C., Lemarechal, C., Sagastizabal, C., 2006. Numerical optimization, theoretical and numerical aspects, 2nd Edition. Springer-Verlag Berlin Heidelberg New York.

Browne, P. A., Wilson, S., 2015. A simple method for integrating a complex model into an ensemble data assimilation system using MPI. Environmental Modelling & Software 68, 122–128.

Broyden, C. G., 1970. The Convergence of a Class of Double-rank Minimization Algorithms 1. General Considerations. IMA Journal of Applied Mathematics 6 (1), 76–90.

Canizares, R., 1999. On the Application of Data Assimilation in Regional Coastal Models. Ph.D. thesis, TU Delft, Delft, Netherlands.

Casulli, V., 1999. A semi-implicit finite difference method for non-hydrostatic, free-surface flows. International Journal for Numerical Methods in Fluids 30 (4), 425–440.

Casulli, V., Cheng, R. T., 1992. Semi-implicit finite difference methods for three-dimensional shallow water flow. International Journal for Numerical Methods in Fluids 15 (6), 629–648.

Casulli, V., Zanolli, P., 2002. Semi-implicit numerical modeling of nonhydrostatic free-surface flows for environmental problems. Mathematical and Computer Modelling 36 (9-10), 1131–1149.

Charney, J. G., Fjörtoft, R., von Neumann, J., 1950. Numerical Integration of the Barotorpic Vorticity Equations. Tellus 2, 237–254.

Clark, M. P., Rupp, D. E., Woods, R. A., Zheng, X., Ibbitt, R. P., Slater, A. G., Schmidt, J., Uddstrom, M. J., 2008. Hydrological data assimilation with the ensemble Kalman filter: Use of streamflow observations to update states in a distributed hydrological model. Advances in Water Resources 31 (10), 1309–1324.

Clayton, A. M., Lorenc, A. C., Barker, D. M., 2013. Operational implementation of a hybrid ensemble/4D-Var global data assimilation system at the Met Office. Quarterly Journal of the Royal Meteorological Society 139 (675), 1445–1461.

Collischonn, W., Haas, R., Andreolli, I., Tucci, C. E. M., 2005. Forecasting River Uruguay flow using rainfall forecasts from a regional weather-prediction model. Journal of Hydrology 305 (1–4), 87–98.

Cosme, E., Brankart, J., Verron, J., Brasseur, P., Krysta, M., 2010. Implementation of a reduced rank square-root smoother for high resolution ocean data assimilation. Ocean Modelling 33 (1–2), 87–100.

Courtier, P., Andersson, E., Heckley, W., Vasiljevic, D., Hamrud, M., Hollingsworth, A., Rabier, F., Fisher, M., Pailleux, J., 1998. The ECMWF implementation of three-dimensional variational assimilation (3D-Var). I: Formulation. Quarterly Journal of the Royal Meteorological Society 124 (550), 1783–1807.

Daescu, N. D., Navon, M. I., 2003. Adaptive observations in the context of 4D-Var data assimilation. Meteorology and Atmospheric Physics 85 (4), 205–226.

Daley, R., 1991. Atmospheric Data Analysis. Cambridge University Press.

Doerffer, R., Schiller, H., 2008. MERIS Lake Water Project – Lake Water Algorithm for BEAM, ATBD 1.0. Algorithm Theoretical Basis Document, 1–17.
URL http://www.brockmann-consult.de/beam-wiki/download/attachments/1900548/ATBD_lake_water_RD20080610.pdf

Drikakis, D., Tsangaris, S., 1993. On the solution of the compressible Navier- Stokes equations using improved flux vector splitting methods. Applied Mathematical Modelling 17 (6), 282–297.

Erpicum, S., Dewals, B., Archambeau, P., Pirotton, M., 2010. Dam break flow computation based on an efficient flux vector splitting. Journal of Computational and Applied Mathematics 234 (7), 2143–2151, fourth International Conference on Advanced COmputational Methods in ENgineering (ACOMEN 2008).

Etherton, B. J., Bishop, C. H., 2004. Resilience of Hybrid Ensemble/3DVAR Analysis Schemes to Model Error and Ensemble Covariance Error. Monthly Weather Review 132 (5), 1065–1080.

Evensen, G., 1992. Using the extended Kalman filter with a multilayer quasi-geostrophic ocean model. Journal of Geophysical Research: Oceans 97 (C11), 17905–17924.

Evensen, G., 1994. Sequential data assimilation with a nonlinear quasi-geostrophic model using Monte Carlo methods to forecast error statistics. Journal of Geophysical Research: Oceans 99 (C5), 10143–10162.

Evensen, G., 1996. Advanced Data Assimilation for Strongly Nonlinear Dynamics. Monthly Weather Review 125 (6), 1342–1354.

Evensen, G., 2004. Sampling strategies and square root analysis schemes for the EnKF. Ocean Dynamics 54 (6), 539–560.

Evensen, G., 2009. Data Assimilation: The Ensemble Kalman Filter, 2nd Edition. Springer-Verlag Berlin Heidelberg.

Evensen, G., van Leeuwen, P. J., 1996. Assimilation of Geosat Data for the Agulhas Current Using Ensemble Kalman Filter with Quasigeostrophic Model. Monthly Weather Review 124 (1), 84–96.

Fertig, E. J., Harlim, J., Hunt, B. R., 2007. A comparative study of 4D-VAR and a 4D Ensemble Kalman Filter: perfect model simulations with Lorenz-96. Tellus A 59 (1), 96–100.

Franssen, H. J. H., Kinzelbach, W., 2008. Real-time groundwater flow modeling with the Ensemble Kalman Filter: Joint estimation of states and parameters and the filter inbreeding problem. Water Resources Research 44 (9), n/a–n/a, W09408.

Fritsch, F. N., Carlson, R. E., 1980. Monotone Piecewise Cubic Interpolation. SIAM Journal on Numerical Analysis 17 (2), 238–246.

Gauthier, P., Charette, C., Fillion, L., Koclas, P., Laroche, S., 1999. Implementation of a 3D variational data assimilation system at the Canadian Meteorological Centre. Part I: The global analysis. Atmosphere-Ocean 37 (2), 103–156.

Gauthier, P., Courtier, P., Moll, P., 1993. Assimilation of Simulated wind Lidar Data with Kalman Filter. Monthly Weather Review 121 (6), 1803–1820.

Gauthier, P., Tanguay, M., Laroche, S., Pellerin, S., Josée, M., 2007. Extension of 3DVAR to 4DVAR: Implementation of 4DVAR at the Meteorological Service of Canada. Monthly Weather Review 135 (6), 2339–2354.

Gauthier, P., Thépaut, J. N., Hollingsworth, A., 1994. A strategy for operational implementation of 4D-Var, using an incremental approach. Quarterly Journal of the Royal Meteorological Society 120 (519), 1367–1387.

Gilbert, J. C., Nocedal, J., 1993. Automatic differentiation and the step computation in the limited memory BFGS method. Applied Mathematics Letters 6 (3), 47–50.

Haario, H., 2006. Statistical Analysis in Modelling: MCMC methods, Ti5416500. Lecture Materials. Department of Information Technology, Lappeenranta University of Technology, Finland.

Hager, W. W., 1989. Updating the Inverse of a Matrix. SIAM Review 31 (2), 221–239.

Hamill, T. M., Snyder, C., 2000. A hybrid ensemble Kalman Filter-3D Variational Analysis Scheme. Monthly Weather Review 128 (8), 2905–2919.

Hamill, T. M., Snyder, C., Morss, R. E., 2000. A comparison of Probabilistic Forecast from bred, Singular-Vector, and Perturbed Observation Ensembles. Monthly Weather Review 128 (6), 1835–1851.

Hamill, T. M., Whitaker, J. S., 2005. Accounting for the Error due to Unresolved Scales in Ensemble Data Assimilation: A Comparison of Different Approaches. Monthly Weather Review 133 (11), 3132–3147.

Hamill, T. M., Whitaker, J. S., Snyder, C., 2001. Distance-Dependent Filtering of Background Error Covariance Estimates in an Ensemble Kalman Filter. Monthly Weather Review 129 (11), 2776–2790.

Heemink, A. W., Metzelaar, I. D. M., 1995. Data assimilation into a numerical shallow water flow model: a stochastic optimal control approach. Journal of Marine Systems 6 (1–2), 145–158, data Assimilation in Marine Science.

Heemink, A. W., Verlaan, M., Segers, A. J., 2001. Variance Reduced Ensemble Kalman Filtering. Monthly Weather Review 129 (7), 1718–1728.

Heniche, M., Secretan, Y., Boudreau, P., Leclerc, M., 2000. A two-dimensional finite element drying-wetting shallow water model for rivers and estuaries. Advances in Water Resources 23 (4), 359–372.

Houtekamer, P. L., Herschel, L. M., 1998. Data Assimilation Using Ensemble Kalman Filter Technique. Monthly Weather Review 126 (3), 796–811.

Houtekamer, P. L., Herschel, L. M., 2001. A sequential Ensemble Kalman Filter for Atmospheric Data Assimilation. Monthly Weather Review 129 (1), 123–137.

Houtekamer, P. L., Herschel, L. M., 2005. Ensemble Kalman filtering. Quarterly Journal of the Royal Meteorological Society 131 (613), 3269–3289.

Hunt, B. R., Kalnay, E., Kostelich, E. J., Ott, E., Patil, D. J., Sauer, T., Szunyogh, I., Yorke, J. A., Zimin, A. V., 2004. Four-dimensional ensemble Kalman filtering. Tellus A 56 (4), 273–277.

Hunt, B. R., Kostelich, E. J., Szunyogh, I., 2007. Efficient data assimilation for spatiotemporal chaos: A local ensemble transform Kalman filter. Physica D: Nonlinear Phenomena 230 (1–2), 112–126, data Assimilation.

Huttula, T., 1994. Suspended Sediment Transport in Lake Säkylän Pyhäjärvi. Aqua Fennica 24 (2), 171–185.

James, G., Burley, D., Clements, D., Dyke, P., Searl, J., Steele, N., Wright, J., 2011. Advanced Modern Engineering Mathematics, 4th Edition. Pearson Education Limited.

Jiashu, Z., Zutao, Z., 2006. Application of a Strong Tracking Finite-Difference Extended Kalman Filter to Eye Tracking. In: Huang, D.-S., Li, K., Irwin, G. (Eds.), Physics of Granular Media. Vol. 4113 of Lecture Notes in Computer Science. Springer Berlin Heidelberg, pp. 1170–1179.

Kalman, R. E., 1960. A New Approach to Linear Filtering and Prediction Problems. Journal of Basic Engineering 82 (1), 35–45.

Kalnay, E., 2003. Atmospheric Modeling, Data Assimilation And Predictability. Cambridge University Press.
URL www.cambridge.org/9780521791793

Kauranne, T., 1992. 4D Variational assimilation, ensemble forecasting and parallel computing. Parallel supercomputing in atmospheric science (Hoffmann, G.-R and Kauranne, T.,eds.). In: Fifth Workshop on the Use of Parallel Processors in Meteorology. World Scientific 1993, pp. 286–311.

Kauranne, T., 1994. Summary of GENESIS work at the European Centre for Medium-range Weather Forecasts (ECMWF). Parallel Computing 20 (10–11), 1685–1688, suprenum and Genesis.

Kauranne, T., 2002. Introducing Parallel Computers into Operational Weather Forecasting. Ph.D. thesis, Lappeenranta University of Technology, Lappeenranta, Finland.

Kim, K., Park, M., Min, J., Ryu, I., Kang, M., Park, L. J., 2014a. Simulation of algal bloom dynamics in a river with the ensemble Kalman filter. Journal of Hydrology 519, Part D, 2810–2821.

Kim, S., Seo, D., Riazi, H., Shin, C., 2014b. Improving water quality forecasting via data assimilation - Application of maximum likelihood ensemble filter to HSPF. Journal of Hydrology 519, Part D, 2797–2809.

Klinker, E., snf G. Kelly, F. R., Mahfouf, J. F., 2000. The ECMWF operational implementation of four-dimensional variational assimilation. III: Experimental results and diagnostics with operational configuration. Quarterly Journal of the Royal Meteorological Society 126 (564), 1191–1215.

Komma, J., Blöschl, G., Reszler, C., 2008. Soil moisture updating by Ensemble Kalman Filtering in real-time flood forecasting. Journal of Hydrology 357 (3–4), 228–242.

Kondrashov, D., Sun, C., Ghil, M., 2008. Data Assimilation for a Coupled Ocean–Atmosphere Model. Part II: Parameter Estimation. Monthly Weather Review 136 (12), 5062–5076.

Le Dimet, F., Talagrand, O., 1986. Variational algorithms for analysis and assimilation of meteorological observations: theoretical aspects. Tellus A 38A (2), 97–110.

Lei, L., Hacker, J. P., 2015. Nudging, Ensemble, and Nudging Ensembles for Data Assimilation in the Presence of Model Error. Monthly Weather Review 143 (7), 2600–2610.

Li, H., Kalnay, E., Miyoshi, T., 2009. Simultaneous estimation of covariance inflation and observation errors within an ensemble Kalman filter. Quarterly Journal of the Royal Meteorological Society 135 (639), 523–533.

Li, L., Zhou, H., Hendricks Franssen, H. J., Gómez-Hernández, J. J., 2012. Groundwater flow inverse modeling in non-MultiGaussian media: performance assessment of the normal-score Ensemble Kalman Filter. Hydrology and Earth System Sciences 16 (2), 573–590.

Li, Z., Chao, Y., McWilliams, J. C., Ide, K., 2008. A Three-Dimensional Variational Data Assimilation Scheme for the Regional Ocean Modeling System. Journal of Atmospheric and Oceanic Technology 25 (11), 2074–2090.

Li, Z., Zang, Z., Li, B. Q., Chao, Y., Chen, D., Ye, Z., Liu, Y., Liou, K. N., 2013. A three-dimensional variational data assimilation system for multiple aerosol species with WRF/Chem and an application to $PM_{2.5}$ prediction. Atmospheric Chemistry and Physics 13 (8), 4265–4278.

Lions, J. L., 1971. Optimal control of systems governed by partial differential equations, 1st Edition. Springer-Verlag Berlin Heidelberg.

Lorenc, A. C., 1986. Analysis methods for numerical weather prediction. Quarterly Journal of the Royal Meteorological Society 112 (474), 1177–1194.

Lorenc, A. C., 1997. Development of an Operational Assimilation Scheme. Journal of the Royal Meteorological Society of Japan 75 (1B), 339–346.

Lorenc, A. C., 2003. The potential of the ensemble Kalman filter for NWP-a comparison with 4D-Var. Quarterly Journal of the Royal Meteorological Society 129 (595), 3183–3203.

Lorenc, A. C., Ballard, S. P., Bell, R. S., abd P. L. F Andrews, N. B. I., Barker, D. M., Bray, J. R., Clayton, A. M., Dalby, T., Li, D., Payne, T. J., Saunders, F. W., 2000. The Met. Office global three-dimensional variational data assimilation scheme. Quarterly Journal of the Royal Meteorological Society 126 (570), 2991–3012.

Lorenc, A. C., Bowler, N. E., Clayton, A. M., Pring, S. R., Fairbairn, D., 2015. Comparison of Hybrid-4DEnVar and Hybrid-4DVar Data Assimilation Methods for Global NWP. Monthly Weather Review 143 (1), 212–229.

Lorenc, A. C., Rawlins, F., 2005. Why does 4D-Var beat 3D-Var? Quarterly Journal of the Royal Meteorological Society 131 (613), 3247–3257.

Lorenz, E., 1996. Predictability: a problem partly solved. In: Seminar on Predictability. Vol. 1. T. Palmer, ed, pp. 1–18.

Lorenz, E., Emanuel, K. A., 1998. Optimal Sites for Supplementary Weather Observations: Simulation with a Small Model. Journal Of The Atmospheric Sciences 55 (3), 399–414.

Luyten, P., 2014. COHERENS – A Coupled Hydrodynamical-Ecological Model for Regional and Shelf Seas: User Documentation. Version 2.6. RBINS Report, Operational Directorate Natural Environment, Royal Belgian Institute of Natural Sciences. COHERENS website.
URL `http://odnature.naturalsciences.be/coherens/manual`

Luyten, P., 2015. Introduction to COHERENS, new features in latest versions. 4th international COHERENS 3-D workshop/seminar and training session. Helsinki, 24–26 November 2015. Lecture Materials.

Luyten, P. J., Jones, J. E., Proctor, R., 2003. A numerical study of the long-and short-term temperature variability and thermal circulation in the North Sea. Journal of Physical Oceanography 33, 37–56.

Lynch, P., 2006. The Emergence of Numerical Weather Prediction. Cambridge University Press.

Madaus, L. E., Hakim, G. J., 2015. Rapid, short-term ensemble forecast adjustment through offline data assimilation. Quarterly Journal of the Royal Meteorological Society 141 (692), 2630–2642.

Madsen, H., Skotner, C., 2005. Adaptive state updating in real-time river flow forecasting-a combined filtering and error forecasting procedure. Journal of Hydrology 308 (1–4), 302–312.

Malve, O., Hjerppe, T., Tattari, S., Väisänen, S., Huttunen, I., Kotamäki, N., Kallio, K., Taskinen, A., Kauppila, P., 2016. Participatory operations model for cost-efficient monitoring and modeling of river basins – A systematic approach. Science of The Total Environment 540, 79–89, 5th Special Issue SCARCE: River Conservation under Multiple stressors: Integration of ecological status, pollution and hydrological variability.

Mano, A., Malve, O., Koponen, S., Kallio, K., Taskinen, A., Ropponen, J., Juntunen, J., Liukko, N., 2015. Assimilation of satellite data to 3D hydrodynamic model of Lake Säkylän Pyhäjärvi. Water Science and Technology 71 (7), 1033–1039.

Martin, N., Gorelick, S. M., 2005. MOD_FreeSurf2D: A MATLAB Surface Fluid Flow Model for Rivers and Streams. Computer & Geosciences 31 (7), 929–946.

Matthies, H., Strang, G., 1979. The solution of nonlinear finite element equations. International Journal for Numerical Methods in Engineering 14 (11), 1613–1626.

Moradkhani, H., Sorooshian, S., Gupta, H. V., Houser, P. R., 2005. Dual state-parameter estimation of hydrological models using ensemble Kalman filter. Advances in Water Resources 28 (2), 135–147.

Nerger, L., 2004. Parallel Filter Algorithms for Data Assimilation in Oceanography. Ph.D. thesis, Universität Bremen.

Nerger, L., Hiller, W., 2013. Software for ensemble-based data assimilation systems-Implementation strategies and scalability. Computers & Geosciences 55, 110–118, ensemble Kalman filter for data assimilation.

Nerger, L., Janjić, T., Schröter, J., Hiller, W., 2012. A Unification of Ensemble Square Root Kalman Filters. Monthly Weather Review 140 (7), 2335–2345.

Nerger, L., Kirchgessner, P., 2015. Building Ensemble-Based Data Assimilation Systems, EGU General Assembly, April 13 - 17, 2015, Vienna, Austria. Geophysical Research Abstracts 17, EGU2015-12170-1.

Nocedal, J., Wright, J. S., 1999. Numerical optimization, 2nd Edition. Springer.

Panofsky, R. A., 1949. Objective Weather-Map Analysis. Journal of Meteorology 6 (6), 386–392.

Pham, D. T., 2000. Stochastic Methods For Sequential Data Assimilation in Strongly Nonlinear Systems. Monthly Weather Review 129 (5), 1194–1207.

Ponsar, S., Luyten, P., 2009. Data assimilation with the EnKF in a 1-D numerical model of a North Sea station. Ocean Dynamics 59 (6), 983–996.

Rabier, F., Courtier, P., 1992. Four-Dimensional Assimilation In the Presence of Baroclinic Instability. Quarterly Journal of the Royal Meteorological Society 118 (506), 649–672.

Räsänen, M., Salonen, V. P., Salo, J., Walls, M., Sarvala, J., 1992. Recent history of sedimentation and biotic communities in Lake Pyhäjärvi, SW Finland. Journal of Paleolimnology 7 (2), 107–126.

Rawlins, F., Ballard, S. P., Bovis, K. J., Clayton, A. M., Li, D., Inverarity, G. W., Lorenc, A. C., Payne, T. J., 2007. The Met Office global four-dimensional variational data assimilation scheme. Quarterly Journal of the Royal Meteorological Society 133 (623), 347–362.

Reichle, R. H., Crow, W. T., Keppenne, C. L., 2008. An adaptive ensemble Kalman filter for soil moisture data assimilation. Water Resources Research 44 (3), n/a–n/a, w03423.

Richardson, L., 1922. Weather Prediction by Numerical Process. Cambridge University Press.

Ruiz, J., Pulido, M., 2015. Parameter Estimation Using Ensemble-Based Data Assimilation in the Presence of Model Error. Monthly Weather Review 143 (5), 1568–1582.

Seif, Z. M., 2015. Variational Ensemble Kalman Filtering in hydrology. Ph.D. thesis, Lappeenranta University of Technology, Lappeenranta, Finland.
URL http://urn.fi/URN:ISBN:978-952-265-833-3

Simon, D., 2002. Training fuzzy systems with the extended Kalman filter. Fuzzy Sets and Systems 132 (2), 189–199.

Simon, D., 2006. Optimal state estimation, Kalman H∞, and nonlinear approaches. Wiley-Interscience.

Smith, P. J., Thornhill, G. D., Dance, S. L., Lawless, A. S., Mason, D. C., Nichols, N. K., 2013. Data assimilation for state and parameter estimation: application to morphodynamic modelling. Quarterly Journal of the Royal Meteorological Society 139 (671), 314–327.

Solonen, A., Bibov, A., Bardsley, J. M., Haario, H., 2014. Optimization-based sampling in ensemble Kalman filtering. International Journal for Uncertainty Quantification 4 (4), 349–364.

Solonen, A., Haario, H., Hakkarainen, J., Auvinen, H., Amour, I., Kauranne, T., 2012. Variational Ensemble Kalman Filtering using Limited Memory BFGS. Electronic Transaction on Numerical Analysis 39, 271–285.

Sun, L., Nistor, I., Seidou, O., 2015. Streamflow data assimilation in SWAT model using Extended Kalman Filter. Journal of Hydrology 531, Part 3, 671–684.

Tippett, M. K., Anderson, J. L., Bishop, C. H., Hamill, T. M., Whitaker, J. S., 2003. Ensemble Square Root Filters. Monthly Weather Review 131 (7), 1485–1490.

Toro, E. F., Vazquez-Cendon, M. E., 2012. Flux splitting schemes for the Euler equations. Computers & Fluids 70, 1–12.

van Leeuwen, P. J., Evensen, G., 1996. Data Assimilation and Inverse Methods in Terms of a Probabilistic Formulation. Monthly Weather Review 124 (12), 2898–2913.

Verlaan, M., Heemink, A. W., 1997. Tidal flow forecasting using reduced rank square root filters. Stochastic Hydrology and Hydraulics 11 (5), 349–368.

Verlaan, M., Heemink, A. W., 2000. Non-linearity in Data Assimilation Applications: A practical Method for Analysis. Monthly Weather Review 129 (6), 1578–1589.

Wan, E. A., Merwe, R. V. D., 2000. The unscented Kalman filter for nonlinear estimation. In: Adaptive Systems for Signal Processing, Communications, and Control Symposium 2000. AS-SPCC. The IEEE 2000. pp. 153–158.

Wang, X., Barker, D. M., Snyder, C., Hamill, T. M., 2008. A Hybrid ETKF-3DVAR Data Assimilation Scheme for the WRF Model. Part I: Observing System Simulation Experiment. Monthly Weather Review 136 (12), 5116–5131.

Wang, X., Hamill, T. M., Whitaker, J. S., Bishop, C. H., 2007. A Comparison of Hybrid Ensemble Transform Kalman Filter-Optimum Interpolation and Ensemble Square Root Filter Analysis Schemes. Monthly Weather Review 135 (3), 1055–1076.

Wei, Z., Li, G., Qi, L., 2006. New quasi-Newton methods for unconstrained optimization problems. Applied Mathematics and Computation 175 (2), 1156–1188.

Whitaker, J. S., Hamill, T. M., 2002. Ensemble data assimilation without perturbed observations. Monthly Weather Review 130, 1913–1924.

Xiao, D., Yang, P., Fang, F., Xiang, J., Pain, C. C., Navon, I. M., 2016. Non-intrusive reduced order modelling of fluid-structure interactions. Computer Methods in Applied Mechanics and Engineering 303, 35–54.

Xiao, Y., Wei, Z., Wang, Z., 2008. A limited memory BFGS-type method for large-scale unconstrained optimization. Computers & Mathematics with Applications 56 (4), 1001–1009.

Xie, X., Zhang, D., 2010. Data assimilation for distributed hydrological catchment modeling via ensemble Kalman filter. Advances in Water Resources 33 (6), 678–690.

Ying, X., Jorgeson, J., Wang, S., 2009. Modeling Dam-Break Flows Using Finite Volume Method on Unstructured Grid. Engineering Applications of Computational Fluid Mechanics 3 (2), 184–194.

Yoon, T., Kang, S., 2004. Finite Volume Model for Two-Dimensional Shallow Water Flows on Unstructured Grids. Journal of Hydraulic Engineering 130 (7), 678–688.

Zhang, D., Lu, Z., Chen, Y., 2007. Dynamic Reservoir Data Assimilation With an Efficient, Dimension-Reduced Kalman Filter. Society of Petroleum Engineers Journal 12 (1), 108–117.

Zhang, F., Zhang, M., Hansen, J. A., 2009a. Coupling ensemble Kalman filter with four-dimensional variational data assimilation. Advances in Atmospheric Sciences 26 (1), 1–8.

Zhang, M., Wu, W. M., 2011. A two dimensional hydrodynamic and sediment transport model for dam break based on finite volume method with quadtree grid. Applied Ocean Research 33 (4), 297–308.

Zhang, X. F., Heemink, A. W., Janssen, L. H. J. M., Janssen, P. H. M., Sauter, F. J., 1999. A computationally efficient Kalman smoother for the evaluation of the CH4 budget in Europe. Applied Mathematical Modelling 23 (2), 109–129.

Zhang, Y., Liu, N., Oliver, D. S., 2009b. Ensemble filter methods with perturbed observations applied to nonlinear problems. Computational Geosciences 14 (2), 249–261.

Zou, X., Navon, I. M., Ledimet, F. X., 1992. An Optimal Nudging Data Assimilation Scheme Using Parameter Estimation. Quarterly Journal of the Royal Meteorological Society 118 (508), 1163–1186.

Zupanski, D., Zupanski, M., 2006. Model Error Estimation Employing an Ensemble Data Assimilation Approach. Monthly Weather Review 134 (5), 1337–1354.

Zupanski, M., 2005. Maximum Likelihood Ensemble Filter: Theoretical Aspects. Monthly Weather Review 133 (6), 1710–1726.

ACTA UNIVERSITATIS LAPPEENRANTAENSIS

669. DE SMET, DIETER. Innovation ecosystem perspectives on financial services innovation. 2015. Diss.

670. PORRAS, PÄIVI. Utilising student profiles in mathematics course arrangements. 2015. Diss.

671. SALMINEN, JUHO. The role of collective intelligence in crowdsourcing innovations. 2015. Diss.

672. ROSAS, SAILA. Co-operative acquisitions – the contextual factors and challenges for co-operatives when acquiring an investor-owned firm. 2015. Diss.

673. SINKKONEN, TIINA. Item-level life-cycle model for maintenance networks – from cost to additional value. 2015. Diss.

674. TUUNANEN, JUSSI. Modelling of changes in electricity end-use and their impacts on electricity distribution. 2015. Diss.

675. MIELONEN, KATRIINA. The effect of cationic-anionic polyelectrolyte multilayer surface treatment on inkjet ink spreading and print quality. 2015. Diss.

676. OMAJENE, JOSHUA. Underwater remote welding technology for offshore structures. 2015. Diss.

677. NUUTINEN, PASI. Power electronic converters in low-voltage direct current distribution – analysis and implementation. 2015. Diss.

678. RUSATSI, DENIS. Bayesian analysis of SEIR epidemic models. 2015. Diss.

679. STRAND, ELSI. Enhancement of ultrafiltration process by pretreatment in recovery of hemicelluloses from wood extracts. 2016. Diss.

680. TANNINEN, PANU. Press forming of paperboard – advancement of converting tools and process control. 2015. Diss.

681. VALTONEN, PETRI. Distributed energy resources in an electricity retailer's short-term profit optimization. 2015. Diss.

682. FORSSTRÖM-TUOMINEN, HEIDI. Collectiveness within start up-teams – leading the way to initiating and managing collective pursuit of opportunities in organizational contexts. 2015. Diss.

683. MAGUYA, ALMASI. Use of airborne laser scanner data in demanding forest conditions. 2015. Diss.

684. PEIPPO, JUHA. A modified nominal stress method for fatigue assessment of steel plates with thermally cut edges. 2015. Diss.

685. MURASHKO, KIRILL. Thermal modelling of commercial lithium-ion batteries. 2016. Diss.

686. KÄRKKÄINEN, TOMMI. Observations of acoustic emission in power semiconductors. 2016. Diss.

687. KURVINEN, EMIL. Design and simulation of high-speed rotating electrical machinery. 2016. Diss.

688. RANTAMÄKI, JUKKA. Utilization of statistical methods for management in the forest industry. 2016. Diss.

689. PANOVA, YULIA. Public-private partnership investments in dry ports – Russian logistics markets and risks. 2016. Diss.

690. BAHARUDIN, EZRAL. Real-time simulation of multibody systems with applications for working mobile vehicles. 2016. Diss.

691. MARTIKAINEN, SOILI. Development and effect analysis of the Asteri consultative auditing process – safety and security management in educational institutions. 2016. Diss.

692. TORVINEN, PEKKA. Catching up with competitiveness in emerging markets – An analysis of the role of the firm's technology management strategies. 2016. Diss.

693. NORONTAUS, ANNUKKA. Oppisopimuskoulutus yritysten tuottamana koulutuspalveluna: tavoitteista vaikutuksiin. 2016. Diss.

694. HALMINEN, OSKARI. Multibody models for examination of touchdown bearing systems. 2016. Diss.

695. TALONPOIKA, ANNA-MARIA. Financial working capital – management and measurement. 2016. Diss.

696. INKINEN, HENRI. Intellectual capital, knowledge management practices and firm performance. 2016. Diss.

697. YANG, XIAOCHEN. Development of a welding production quality control and management system model for China. 2016. Diss.

698. LEMINEN, VILLE. Leak-proof heat sealing of press-formed paperboard trays. 2016. Diss.

699. LAAKSONEN, LAURI. Spectral retinal image processing and analysis for ophthalmology. 2016. Diss.

700. OINONEN, MINNA. Management of customer co-development in business-to-business markets. 2016. Diss.

701. ALATALO, SARA-MAARIA. Hydrothermal carbonization in the synthesis of sustainable porous carbon materials. 2016. Diss.

702. UZHEGOV, NIKITA. Design and material selection of high-speed rotating electrical machines. 2016. Diss.

703. RICHTER, CHRIS. Digital collaborations and entrepreneurship – the role of shareconomy and crowdsourcing in the era of smart city. 2016. Diss.

704. JAFARI, SHILA. Investigation of adsorption of dyes onto modified titanium dioxide. 2016. Diss.

705. PATEL, YOGINI. Computational modelling of non-equilibrium condensing steam flows in low-pressure steam turbines. 2016. Diss.

706. LEVCHUK, IRINA. Titanium dioxide based nanomaterials for photocatalytic water treatment. 2016. Diss.